aerospace

MDPI

Article

Decision Science Driven Selection of High-Temperature Conventional Ti Alloys for Aeroengines

Ramachandra Canumalla [1,*,†] and Tanjore V. Jayaraman [2,*,†]

1 Weldaloy Specialty Forgings, Warren, MI 48089, USA
2 Department of Mechanical Engineering, University of Michigan-Dearborn, Dearborn, MI 48128, USA
* Correspondence: r.canumalla@weldaloy.com (R.C.); tvjraman@umich.edu (T.V.J.)
† These authors contributed equally to this work.

Abstract: Near-α Ti alloys find themselves in advanced aeroengines for applications of up to 600 °C, mainly as compressor components owing to their superior combination of ambient- and elevated-temperature mechanical properties and oxidation resistance. We evaluated, ranked, and selected near-α Ti alloys in the current literature for high-temperature applications in aeroengines driven by decision science by integrating multiple attribute decision making (MADM) and principal component analysis (PCA). A combination of 12 MADM methods ranked a list of 105 alloy variants based on the thermomechanical processing (TMP) conditions of 19 distinct near-α Ti alloys. PCA consolidated the ranks from various MADMs and identified top-ranked alloys for the intended applications as: Ti-6.7Al-1.9Sn-3.9Zr-4.6Mo-0.96W-0.23Si, Ti-4.8Al-2.2Sn-4.1Zr-2Mo-1.1Ge, Ti-6.6Al-1.75Sn-4.12Zr-1.91Mo-0.32W-0.1Si, Ti-4.9Al-2.3Sn-4.1Zr-2Mo-0.1Si-0.8Ge, Ti-4.8Al-2.3Sn-4.2Zr-2Mo, Ti-6.5Al-3Sn-4Hf-0.2Nb-0.4Mo-0.4Si-0.1B, Ti-5.8Al-4Sn-3.5Zr-0.7Mo-0.35Si-0.7Nb-0.06C, and Ti-6Al-3.5Sn-4.5Zr-2.0Ta-0.7Nb-0.5Mo-0.4Si. The alloys have the following metallurgical characteristics: bimodal matrix, aluminum equivalent preferably ~8, and nanocrystalline precipitates of Ti_3Al, germanides, or silicides. The analyses, driven by decision science, make metallurgical sense and provide guidelines for developing next-generation commercial near-α Ti alloys. The investigation not only suggests potential replacement or substitute for existing alloys but also provides directions for improvement and development of titanium alloys over the current ones to push out some of the heavier alloys and thus help reduce the engine's weight to gain advantage.

Keywords: near-α Ti alloys; aeroengine applications; multiple attribute decision making

Citation: Canumalla, R.; Jayaraman, T.V. Decision Science Driven Selection of High-Temperature Conventional Ti Alloys for Aeroengines. *Aerospace* **2023**, *10*, 211. https://doi.org/10.3390/aerospace10030211

Academic Editor: Sebastian Heimbs

Received: 10 February 2023
Revised: 22 February 2023
Accepted: 22 February 2023
Published: 24 February 2023

1. Introduction and Background

The selection of materials for aeroengine applications to meet the stringent requirements of high specific strength, good creep and fatigue resistance, high fracture toughness, oxidation and corrosion resistance, and so forth, is a challenge. To explore suitable materials for applications, including compressor blades, at temperatures of up to ~500 °C, an effort to select materials using Cambridge Engineering Selector (CES) software was attempted by maximizing several material performance indices, such as resistance to bending, fatigue, specific stiffness, and so on [1]. The analysis revealed titanium (Ti) alloys provide the best performance in temperatures of up to ~500 °C considering the cost and other trade-offs among the other competing alloy systems, viz., low alloy steels, stainless steels, nickel-based superalloys, etc. However, once the selection is zoomed down to Ti alloys, as per the analyses in [1], it is imperative to focus on the choice of apt Ti alloys for applications where strength-efficient structures and corrosion resistance are immanent, including aeroengines [2].

Since the beginning of the historical evolution in 1954, the high-temperature conventional Ti alloys, also known as near-α Ti alloys [3–8], are the choice class among the five different categories of Ti alloys for applications in compressor components in temperatures of up to ~600 °C in aeroengines [9,10]. The most advanced current commercial near-α

Ti alloys are IMI834 and Ti-1100, with the capability for applications up to ~600 °C [11,12]. However, several investigations have shown that low tensile ductility at room temperature is a concern, which is attributed to various reasons, such as the precipitation of silicides, silicides aided by Ti_3Al, Ti_3Al aided by silicides, Ti_3Al, etc. [3]. Therefore, alternative thermomechanical processing (TMP) and stability of the microstructures in service conditions are currently being investigated to mitigate the low tensile ductility at room temperature (that is designer specific) in near-α Ti alloys, which is critical for compressor components in aeroengines. The standard processing condition for the most current commercial alloy (IMI 834), suitable for up to ~600 °C, is typically considered the benchmark. However, generating creep, fatigue, fracture toughness, etc., obtaining data for the intended application/s on every one of those alternatives and variations become time-consuming, tedious, and expensive. Thus, to advance research and perform testing in a limited, faster, less expensive, and more sensible way, it is necessary to sort and select a few alloys, among the several alternative alloys available in the current literature, based on the important and easy to obtain room temperature tensile properties, by adopting decision science driven methods.

Material selection, a holistic approach of selecting an optimal material from a list of materials that is best suited for a given design and application, typically involves compromises between various material properties (mechanical, physical, chemical, etc.), cost, availability, environmental effects, to name a few [13]. The most common approach to material selection is Ashby's material-selection approach—popularly referred to as the materials property chart approach [13–15]. The less common techniques include multiple attribute decision making (MADM) [16–23], cost per unit property method [15,24], Pareto-optimal solutions [15], and artificial intelligence methods (e.g., neural networks) [15,25,26]. MADM refers to making preference decisions over the available alternatives (list of materials) characterized by multiple, usually conflicting attributes (i.e., properties) [22,23]. MADM techniques find applications widely in various industries, including but not limited to logistics, management, manufacturing, and so on [27]. In this paper, we compile, evaluate, sort, and select near-α Ti alloys in the current literature for high-temperature applications in aeroengines, driven by decision science integrating MADM and principal component analysis (PCA). A combination of 12 MADM methods ranks a list of 105 alloy variants based on the TMP conditions of 19 different near-α Ti alloys (the majority are 'research' alloys). PCA, a powerful tool that transforms a multi-dimensional dataset into two dimensions [28–30], consolidates the ranks from various MADMs and identifies the ten top-ranking alloy variants for the intended applications.

2. Methods

Figure 1 presents a flowchart of the decision science driven selection of near-α Ti alloys from the literature for applications in compressor parts in aeroengines. The literature data comprises 105 variants (based on the TMP routes) of 19 distinct near-α Ti alloys. The method consists of three key routines: (i) Literature data (compilation of the near-α Ti alloys), (ii) Ranking (ranking by MADM methods), and (iii) Analyses (rank consolidation by PCA and interpretation).

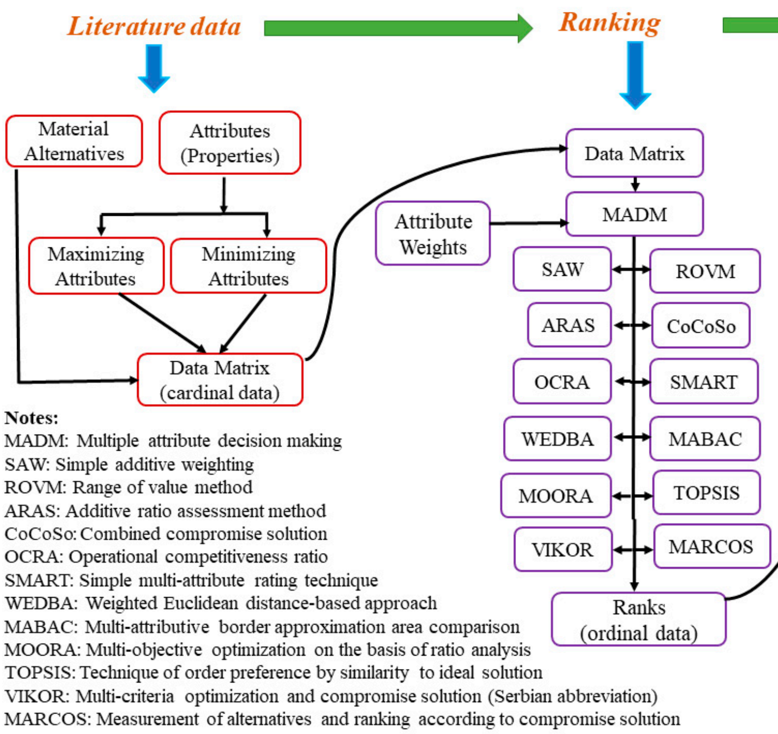

Figure 1. The flowchart of decision science driven analyses of the near-α Ti alloys. It comprises three routines: literature data, ranking, and analyses.

2.1. Literature Data

We compiled a list of near-α Ti alloys (alternatives) and their room-temperature mechanical properties (attributes) from the literature. Table A1 (in Appendix A) presents the alternatives, the near-α Ti alloys, screened for the current study primarily from peer-reviewed journals and conference proceedings [31–52]. The table presents the nominal chemistry, processing conditions, and imminent microstructure. Eleven of the above 19 alloys are 'research' alloys (viz., WJZ-Ti, KIMS, JZ1, JZ2, JL, LD-Ti423, TMC-Ti213, TKT-1, TKT-2, TKT-3, and PC), implying they were fabricated and processed on a laboratory scale (under development) followed by characterization and testing. Eight of the 19 are current commercial alloys (IMI685, IMI829, IMI834, Ti-1100, Ti6242S, TA19, TA29, and Ti60). We identified room temperature % elongation (%*EL*), yield strength (*YS*), and ultimate tensile strength (*UTS*) as the properties (attributes) for the current investigation. For a targeted application, such as the compressor blade, the material needs to satisfy the desired room-temperature attributes (i.e., %*EL*, *YS*, and *UTS*) before examining the other important attributes, namely, the high-temperature properties, including creep resistance, oxidation resistance, and corrosion resistance to optimize the alloy. In the parlance of MADM, all of the identified attributes (%*EL*, *YS*, and *UTS*) are maximizing (or beneficial) attributes, suggesting, for most applications, that the alloys ought to have the following combination: high %*EL*, high *YS*, and high *UTS*. Table A2 (in Appendix A) is the decision matrix comprising the alternatives (near-α Ti alloys) and attributes (properties %*EL*, *YS*, and *UTS*) in the literature [31–52].

2.2. Ranking

We evaluated the decision matrix (Table A2) by several multiple MADM methods. MADM refers to making preference decisions by evaluating and prioritizing alternatives on multiple attributes [22,23]. Distinct components of the MADM are (i) the decision matrix, which comprises the alternatives and the attributes, and (ii) attribute weights: the priorities of attributes are expressed quantitatively according to the MADM theory—they quantify the relative importance of each of the attributes [22,23,53]. The attribute weights are typical of three types [53]: (a) objective weights—based on the decision matrix utilizing mathematical models without considering the decision maker's preferences (e.g., mean weighing, standard deviation method, entropy, etc.), (b) subjective weights, based on the preference derived from the evaluations of the experts (from their previous experience) or designers (constraints of design), or both, and (c) integrated weights, as the name suggests, both objective and subjective weighting are combined to determine the weights. We adopted objective and subjective attribute weights in this investigation.

We evaluated the weights by assigning equal weights (1/3) for each of the attributes based on the understanding of these materials and their intended application. We identified twelve MADM methods to evaluate the data matrix and rank the alloys, including the simple additive weighting (SAW) [22,23,53–55], range of value method (ROVM) [56,57], additive ratio assessment method (ARAS) [58–60], combined compromise solution (CoCoSo) [61–63], operational competitiveness ratio (OCRA) [64–66], simple multi-attribute rating technique (SMART) [22,53,67,68], weighted Euclidean distance-based approach (WEDBA) [23,69,70], multi-attributive border approximation area comparison (MABAC) [71,72], multi-objective optimization on the basis of ratio analysis (MOORA) [73,74], technique of order preference by similarity to ideal solution (TOPSIS) [22,53,75,76], multi-criteria optimization and compromise solution (VIKOR)—the Serbian name is VIse Kriterijumska Optimizacija Kompromisno Resenje—method [77–79], and measurement of alternatives and ranking according to compromise solution (MARCOS) [80,81]. Each MADM approach comprises a unique mathematical aggregation procedure to rank the alternatives. The MADMs identified were diverse. Applying such distinct aggregation procedures is likely to generate a robust set of ranks of the alternatives. The ranks produced by each method, as would be expected, are likely to deviate from one another; nevertheless, the correlation among the various techniques is expected to strengthen the reliability of the results. The modus operandi was soft coded in Microsoft Excel, as formulated in the respective references of MADMs.

2.3. Analyses

The ranks obtained by various MADMs were correlated. We evaluated Spearman's correlation coefficients [82,83] among the ranks obtained from the 12 MADMs. We consolidated the ranks from various MADMs by estimating their mean and by principal component analysis (PCA). PCA, a multivariate technique, reduces the dimensionality of a dataset consisting of several interrelated variables by transforming to a new set of variables termed the principal components (PCs), which are uncorrelated and are ordered so that the first few PCs (typically one or two) retain most of the variation present in the original data [28,29]. The score plot presents a visual representation of the rank evaluation. The analyses were carried out using the commercial software Minitab® 20.

3. Results and Discussions

Figure 2 presents the ranks of the near-α Ti alloys from the literature evaluated by the 12 MADMs. The ranks of the alloys represented as points in the figure by nature are discrete; thin dotted lines for a better visual effect connect the ranks assessed by each of the MADMs. Despite the unique mathematical aggregation procedures in various MADMs, the peaks and troughs of several MADMs somewhat coincide. For example, several MADMs assign similar ranks to WJZ-Ti-2, TKT-2, WJZ-Ti-1, PC-IMDF4, and KIMS-2 (green-shaded). Moreover, the rank assigned by various MADMs to most alloys differs significantly, for instance, as in the alloys designated as Ti-1100-5, IMI834-5 and JZ2-3 (pink shaded). Table 1 presents the Spearman rank (S_ρ) that correlates ranks evaluated by the 12 MADMs. For example, the S_ρ between CoCoSo and ROVM, MABAC and WEDBA, or MARCOS and TOPSIS is >0.95, which indicates strong correlations. On the contrary, S_ρ between ARAS and SMART or TOPSIS and SMART is less than <0.3, which is expected owing to the distinct mathematical aggregation formulation in various MADMs. Out of the 66 combinations of MADM pairs, ~72% have rank correlations equal to or above 0.70, which elicits the robustness and validity of the ranking of the near-α Ti alloys. Therefore, it is imperative to consolidate the ranks obtained from various MADMs. Based on S_ρ among all various combinations of MADMs, it is practical to consolidate the rankings evaluated by the 12 different MADM evaluations. Accordingly, the mean-based (arithmetic mean) rank consolidation of Figure 2 is shown in Figure 3. The ranks of the top ten data points are WJZ-Ti-2, WJZ-Ti-1, TKT-2, TA19-2, TKT-6, TKT-1, TA19-1, KIMS-2, IMI834-2, and PC-IMDF4 in that order.

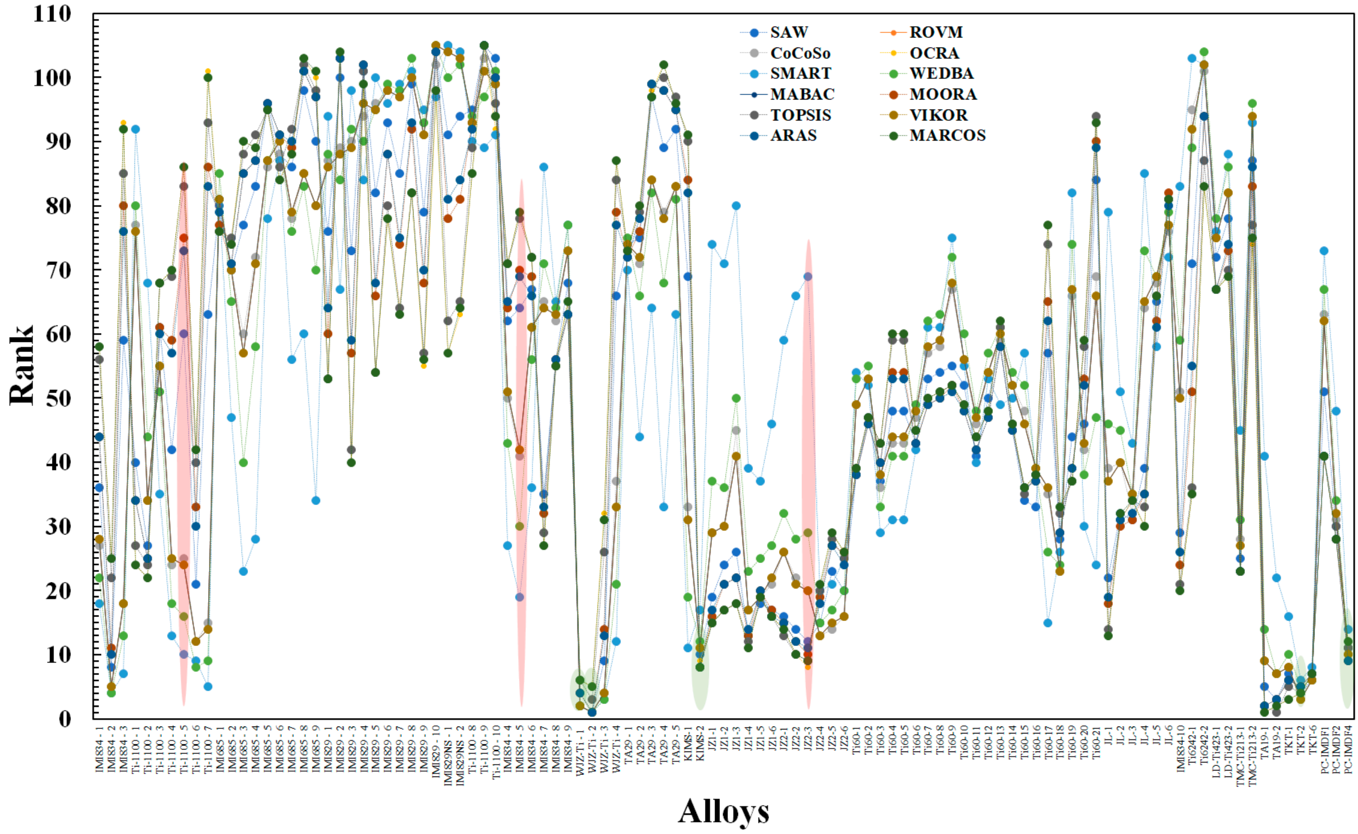

Figure 2. The ranks of the near-α Ti alloys from the literature evaluated by the 12 multiple attribute decision making (MADM) methods. Several MADMs assign relatively similar ranks (green shaded) to WJZ-Ti-2, TKT-2, WJZ-Ti-1, PC-IMDF4, and KIMS-2, while Ti-1100-5, IMI834-5, and JZ2-3 are assigned diverse set of ranks (pink shaded).

Table 1. The Spearman rank (S_ρ) correlation of the near-α Ti alloys ranks from the literature evaluated by the 12 multiple attribute decision-making (MADM) methods.

	SAW	*ROVM*	*CoCoSo*	*OCRA*	*SMART*	*WEDBA*	*MABAC*	*MOORA*	*TOPSIS*	*VIKOR*	*ARAS*
ROVM	0.902										
CoCoSo	0.903	0.999									
OCRA	0.906	0.661	0.660								
SMART	0.530	0.799	0.800	0.172							
WEDBA	0.826	0.983	0.981	0.544	0.884						
MABAC	0.902	1.000	0.999	0.661	0.799	0.983					
MOORA	0.973	0.794	0.794	0.975	0.357	0.694	0.794				
TOPSIS	0.925	0.698	0.696	0.998	0.216	0.584	0.698	0.984			
VIKOR	0.902	1.000	0.999	0.661	0.799	0.983	1.000	0.794	0.698		
ARAS	0.980	0.813	0.812	0.967	0.383	0.716	0.813	0.999	0.978	0.813	
MARCOS	0.907	0.665	0.663	1.000	0.176	0.548	0.665	0.976	0.998	0.665	0.968

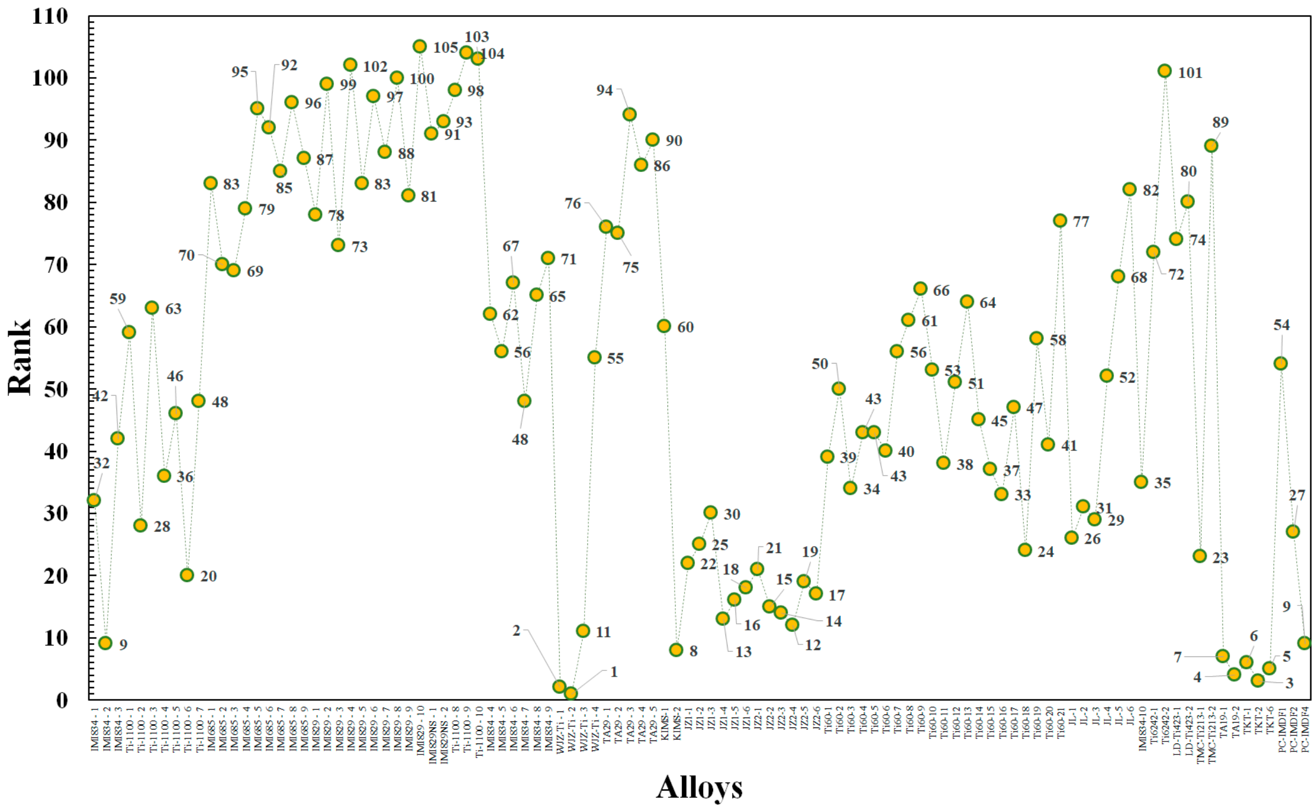

Figure 3. The arithmetic mean-based rank consolidation of the near-α Ti alloys from the literature evaluated by the 12 multiple attribute decision making (MADM) methods. The ranks of the top 10 data points are WJZ-Ti-2, WJZ-Ti-1, TKT-2, TA19-2, TKT-6, TKT-1, TA19-1, KIMS-2, IMI834-2, and PC-IMDF4 in that order.

Figure 4 is the score plot that presents the consolidated rank by PCA, of the near-α Ti alloys. It is the plot of the first two components (*PC1* and *PC2*), post-reduction of the data dimensionality (i.e., ranks from 12 MADMs) into a two-dimensional space. Table 2 presents the eigenvalues (and their proportion) that capture the variation of the distribution of each principal component. The first principal component (*PC1*) captures ~82% of the variation or scatter in the original data, while the second principal (*PC2*) describes ~17% of the variation. Since *PC1* captures nearly 82% of the variation in the initial 12 dimensions (sets of ranks), it approximates the rank of near-α Ti alloys. An imaginary reference line perpendicular to *PC1* traversing from left to right (−6 to 6) indicates the overall ranks of the near-α Ti alloys. The alloy grades WJZ-Ti, TKT-2, TA19, TKT-6, TKT-1, KIMS, IMI834, and PC top the list, followed by JZ1, JZ2, Ti-1100, and so on. The ranks of the top ten data points are WJZ-Ti-2, WJZ-Ti-1, TKT-2, TA19-2, TKT-6, TKT-1, TA19-1, KIMS-2, IMI834-2, and PC-IMDF4 in that order (the data points within the box in Figure 4), while certain variants of WJZ-Ti, JZ1, and JZ2 also appear promising (the data points close to the box). The top-ranked alloys by PCA-based consolidation are strikingly similar to the top-ranked alloys evaluated by mean-based consolidation. Specifically, the PCA-based consolidation refines the IMI834-2 (rank#9) and PC-IMDF4 (rank#9) assigned by mean-based consolidation to rank#9 and #10, respectively. Therefore, it is logical to label the score plot of PCA-based consolidated ranks as a 'rank chart'.

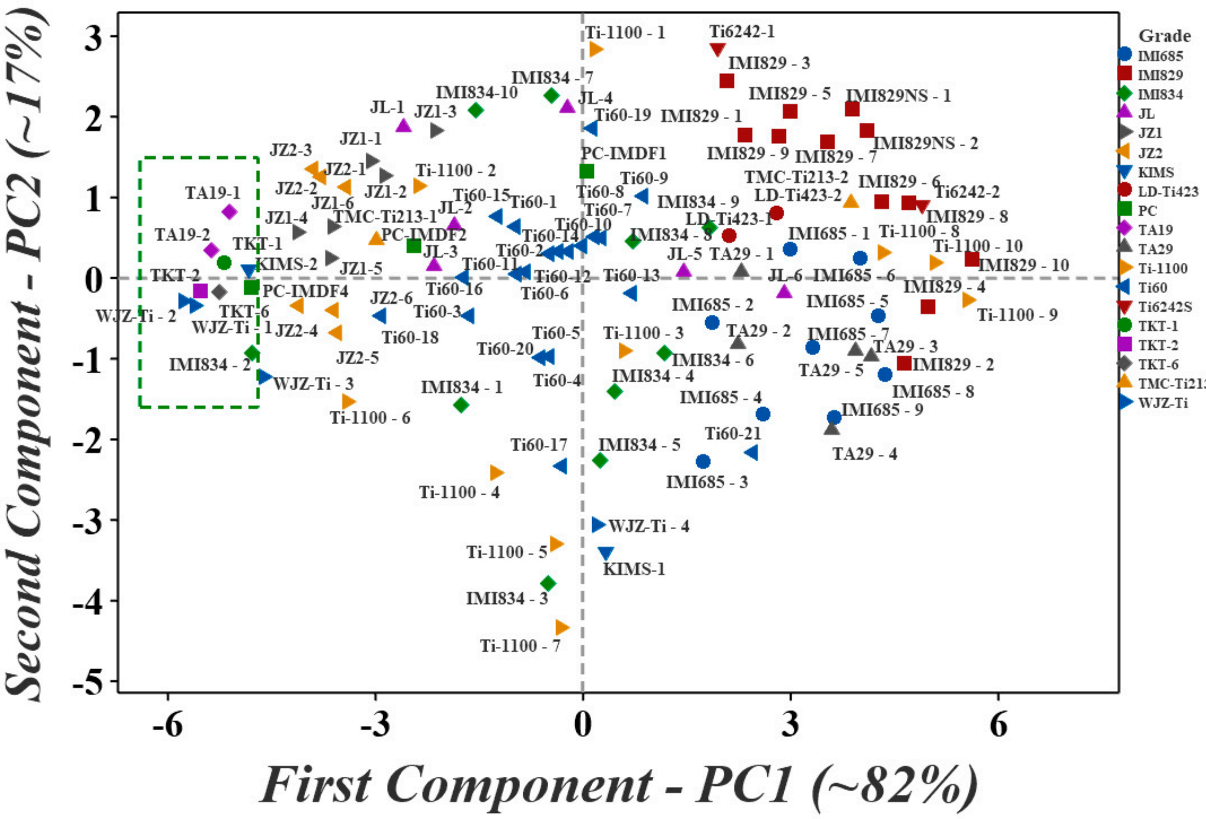

Figure 4. Score plot by principal component analysis (PCA) of the ordinal data, i.e., PCA-based rank consolidation of the near-α Ti alloys evaluated by the 12 MADM methods. The top-ranked alloy variants evaluated by PCA-based consolidation are strikingly similar to the top-ranked alloy variants evaluated by the mean-based consolidation. Specifically, the PCA-based consolidation refines the IMI834-2 (rank#9) and PC-IMDF4 (rank#9) assigned by the mean-based consolidation to rank#9 and #10, respectively.

Table 2. The eigenvalues and their proportion by the principal component analysis (PCA) of the ranks of the near-α Ti alloys from the literature by the 12 multiple attribute decision making (MADM) methods.

	PC1	*PC2*	*PC3*	*PC4*	*PC5*	*PC6*	*PC7*	*PC8*	*PC9*	*PC10*	*PC11*	*PC12*
Eigenvalue	9.833	2.044	0.089	0.022	0.005	0.003	0.002	0.001	0.000	0.000	0.000	0.000
Proportion	0.819	0.170	0.007	0.002	0.000	0.000	0.000	0.000	0.000	0.000	0.000	0.000
Cumulative	0.819	0.990	0.997	0.999	1.000	1.000	1.000	1.000	1.000	1.000	1.000	1.000

For deeper insight into the rank chart (Figure 4) of near-α Ti alloys, Figure 5a–d presents the score plots through the lens of various categories. Here, the region of interest (green box) corresponds to the top 10 alloy variants. Key inferences from the figures are as follows: (i) majority (seven out of 10) of the data points in the area of interest have aluminum equivalent to 8 (Figure 5a), (ii) all of the data points in the region of interest have a bimodal matrix, i.e., primary α + transformed β (Figure 5b), (iii) among the top ten data points, five (WJZ-Ti-1, TKT-2, TKT-1, TA19-2, and TA19-1) have no precipitates; one of them, WJZ-Ti-2, has precipitates Ti_3Al in αp-1 (inside primary α); one of them (TKT-6) has germanide precipitates; one has silicide precipitates (KIMS-2—Hf in silicide and no Zr); and two (IMI834-2 and PC-IMDF4) have no information regarding the precipitates (Figure 5c) based on the chemistry, thermomechanical processing and the thermal treatments, these two variants would highly likely have Ti_3Al and silicides; and lastly (iv) among the top 10 data points, five have no precipitates, four of them have nanocrystalline precipitates, and one has no information about any precipitate (Figure 5d). These analyses suggest guidelines for developing next-generation commercial near-α Ti alloys. The alloy design strategy for near-α Ti alloys for high-temperature applications with a combination of high YS, high UTS, and high $\%EL$ has two distinct options: (i) a combination of the aluminum equivalent to 8 and a bimodal matrix (primary α + transformed β) with no precipitates, (ii) a combination of the aluminum equivalent to 8, bimodal matrix, and nanocrystalline Ti_3Al or germanide or silicide (no Zr, but Hf, as the silicides containing Hf, do not reduce ductility, however, Hf provides solid solution strengthening [3]) precipitates in α.

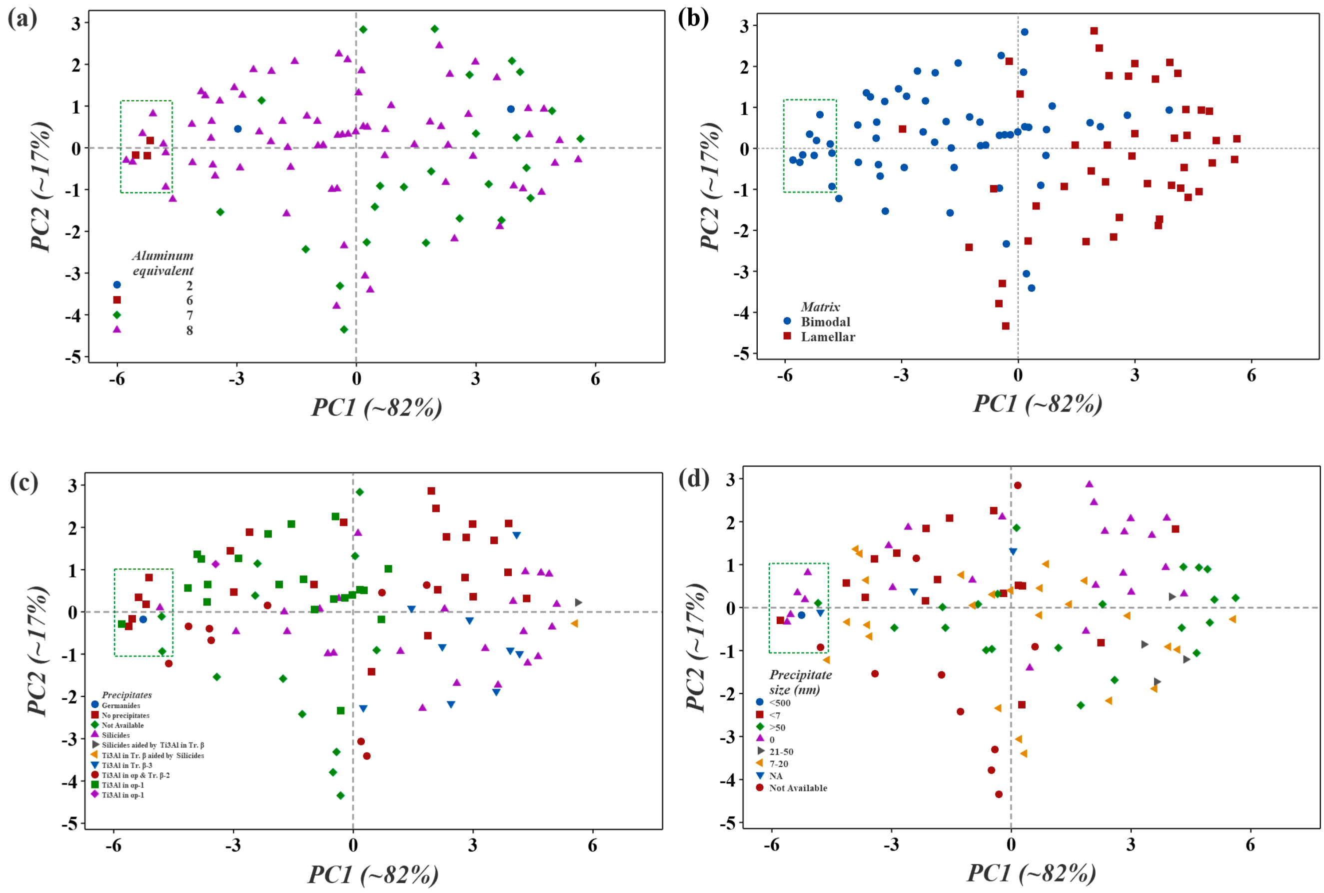

Figure 5. Score plots by the principal component analysis (PCA) of the ordinal data, i.e., PCA-based rank consolidation of the near-α Ti alloys evaluated by the 12 MADM methods through the lens of, i.e., categorized based on (**a**) aluminum equivalent, (**b**) matrix, (**c**) precipitates, and (**d**) precipitate size. The region of interest (green box) shows the top-ranked ten alloy variants.

In this investigation, we compile, evaluate, sort, and select near-α Ti alloys in the current literature for high-temperature applications in aeroengines, driven by decision science, by integrating MADM and principal component analysis (PCA). The evaluation provided valuable insight into potential existing materials ('research alloys') to focus on further research and development for commercialization. Among the top-ranked ten alloy variants (WJZ-Ti-2, WJZ-Ti-1, TKT-2, TA19-2, TKT-6, TKT-1, TA19-1, KIMS-2, IMI834-2, and PC-IMDF4), seven variants belong to the six 'research grade' alloys (WJZ-Ti, TKT-2, TKT-6, TKT-1, KIMS, and PC), while the data point IMI834-2 is a variant of an existing commercial alloy IMI834. Thus, all of these alloys appear to be strong contenders for large-scale development and testing. Additionally, in the future, newly discovered novel high-temperature Ti alloys (conventional and high-entropy alloys) can be included in the list and evaluated to assess their relative position in the rank chart and infer their potential to replace existing materials. In the near future, we plan to expand the decision science driven material selection by including several other relevant mechanical properties as they become available. Lastly, this effort (i) validates the decision science driven MADM coupled with PCA for sorting, ranking, and material selection, (ii) weeds out the alloys that need not be pursued further with time-consuming experimental studies to generate data on additional attributes that are required for use for the intended application/s, and (iii) provide directions for advancing alloys that are under development or suggest some critical improvements for possible newer alloys by providing metallurgical perspectives. Developing a methodology that applies decision science principles to compile and sort a relatively large literature data, select or identify top-ranked alloys, unearth metallurgical patterns, and recommend guidelines for developing next-generation commercial near-α Ti alloys for aeroengines is the novelty of the investigation.

4. Summary and Conclusions

We compiled, evaluated, ranked, and selected near-α Ti alloys in the current literature for high-temperature applications in aeroengines, driven by decision science by integrating MADM and principal component analysis (PCA). A combination of 12 MADM methods ranked a list of 105 alloy variants based on the thermomechanical processing (TMP) conditions of 19 different near-α Ti alloys. PCA consolidated the ranks from various MADMs and identified ten top-ranked alloy variants for the intended application/s. The ten top-ranked alloy variants are WJZ-Ti-2, WJZ-Ti-1, TKT-2, TA19-2, TKT-6, TKT-1, TA19-1, KIMS-2, IMI834-2, and PC-IMDF4 in that order and they correspond to the following eight alloys: Ti-6.7Al-1.9Sn-3.9Zr-4.6Mo-0.96W-0.23Si, Ti-4.8Al-2.2Sn-4.1Zr-2Mo-1.1Ge, Ti-6.6Al-1.75Sn-4.12Zr-1.91Mo-0.32W-0.1Si, Ti-4.9Al-2.3Sn-4.1Zr-2Mo-0.1Si-0.8Ge, Ti-4.8Al-2.3Sn-4.2Zr-2Mo, Ti-6.5Al-3Sn-4Hf-0.2Nb-0.4Mo-0.4Si-0.1B, Ti-5.8Al-4Sn-3.5Zr-0.7Mo-0.35Si-0.7Nb-0.06C, and Ti-6Al-3.5Sn-4.5Zr-2.0Ta-0.7Nb-0.5Mo-0.4Si. The top-ranked alloys evaluated by PCA-based consolidation are strikingly similar to the top-ranked alloys evaluated by mean-based consolidation. The top-ranked alloys suggest the following metallurgical characteristics: bimodal matrix (primary α + transformed β), aluminum equivalent preferably up to 8, and nanocrystalline precipitates of Ti_3Al, germanides, or silicides. The analyses driven by decision science made metallurgical sense. It provides guidelines for developing next-generation commercial near-α Ti alloys. The alloy design strategy for near-α Ti alloys for high-temperature applications with a combination of high YS, high UTS, and high $\%EL$ has two distinct options: (i) a combination of the aluminum equivalent to 8 and a bimodal matrix with no precipitates, or (ii) a combination of the aluminum equivalent to 8, bimodal matrix, and nanocrystalline Ti_3Al or germanide or silicide (not Zr, but Hf, as the silicides containing Hf do not reduce ductility, to the contrary, Hf provides solid solution strengthening) precipitates in α. Thus, novel alloys could be developed based on these directions for the future. A similar analysis could include data from newer exotic experimental materials, such as composites, for compressor parts.

Author Contributions: Conceptualization, T.V.J. and R.C.; Methodology, T.V.J.; Software, T.V.J.; Validation, R.C. and T.V.J.; Formal Analysis, T.V.J. and R.C.; Investigation, T.V.J. and R.C.; Data Curation, R.C.; Writing—Original Draft Preparation, T.V.J.; Writing—Review & Editing, T.V.J. and R.C.; Visualization, T.V.J.; Supervision, R.C. and T.V.J.; Project Administration, R.C. and T.V.J.; Funding Acquisition, R.C. and T.V.J. All authors have read and agreed to the published version of the manuscript.

Funding: Weldaloy Specialty Forgings (Research and Development Account# 8860.00) Institute of Advanced Vehicle Systems (grant# 052349), University of Michigan-Dearborn.

Institutional Review Board Statement: Not applicable.

Informed Consent Statement: No applicable.

Data Availability Statement: The data used in the analyses is presented in Tables A1 and A2.

Acknowledgments: The author R. Canumalla thanks the Weldaloy Specialty Forgings management for all their support; the author T. V. Jayaraman, thanks the Department of Mechanical Engineering, College of Engineering and Computer Science, University of Michigan-Dearborn for all their support.

Conflicts of Interest: The authors declare no conflict of interest.

Appendix A

Table A1. The alternatives, a list of 105 variants of 19 distinct near-α Ti alloys identified for the investigation, chemistry (nominal composition), fabrication and processing conditions, and microstructure; alloy designation is the unique identifier assigned to the variants.

Sl#	*Alloy*	*Chemistry (Nominal)*	*Processing Step 1*	*Processing Step 2*	*Microstructure Description*	*Alloy Designation*	*Ref.*
1	IMI834	Ti-5.8Al-4Sn-3.5Zr-0.7Mo-0.35Si-0.7Nb-0.06C	834-(α + β)ST1025 °C OQ	700 °C	Micro 1-Bimodal-αp (15 vol.%/15–20 µm) & Tr.β	IMI834-1	[31]
2	IMI834	Ti-5.8Al-4Sn-3.5Zr-0.7Mo-0.35Si-0.7Nb-0.06C	834-TMT-(α + β)ST1000WQ	600 °C-4 h	Micro 2-Bimodal-higher amount of αp than Micro1	IMI834-2	[31]
3	IMI834	Ti-5.8Al-4Sn-3.5Zr-0.7Mo-0.35Si-0.7Nb-0.06C	834-TMT-βST1080 °C WQ	600 °C-4 h	Micro 3-Lamellar-Tr.β	IMI834-3	[31]
4	Ti-1100	Ti-5.8Al-2.7Sn-4Zr-0.4Mo-0.45Si	Ti-1100 °C Forged at 980 °C AQ	Unaged	Micro A-Bimodal-αp (15 vol.%/15–20 µm) & Tr.β	Ti-1100-1	[31]
5	Ti-1100	Ti-5.8Al-2.7Sn-4Zr-0.4Mo-0.45Si	Ti-1100 °C (α + β) ST940 °C WQ	600 °C-4 h	Micro B-Bimodal and finer than Micro A	Ti-1100-2	[31]
6	Ti-1100	Ti-5.8Al-2.7Sn-4Zr-0.4Mo-0.45Si	Ti-1100 °C (α + β) ST980 °C WQ	600 °C-4 h	Micro C-Bimodal coarse compared to Micro B but comparable to Micro-A	Ti-1100-3	[31]
7	Ti-1100	Ti-5.8Al-2.7Sn-4Zr-0.4Mo-0.45Si	Ti-1100 °C-βST1020 °C WQ	600 °C-4 h	Micro D-Lamellar-Prior β grain size 200 µm	Ti-1100-4	[31]
8	Ti-1100	Ti-5.8Al-2.7Sn-4Zr-0.4Mo-0.45Si	Ti-1100 °C-βST1060WQ	600 °C-4 h	Micro E-Lamellar-Prior β grain size 500 to 600 µm	Ti-1100-5	[31]
9	Ti-1100	Ti-5.8Al-2.7Sn-4Zr-0.4Mo-0.45Si	Ti-1100 °C-TMT-(α + β) ST1000 °C WQ	600 °C-4 h	Micro F-Bimodal-finer compared to Micro C	Ti-1100-6	[31]
10	Ti-1100	Ti-5.8Al-2.7Sn-4Zr-0.4Mo-0.45Si	Ti-1100 °C-TMT-βST1060 °C WQ	600 °C-4 h	Micro G-Lamellar-finer compared to Micro E	Ti-1100-7	[31]
11	IMI685	Ti-6.18Al-5.27Zr-0.5Mo-0.28Si	685-βST1050 °C-WQ	Unaged	Lamellar α'—No precipitates	IMI685-1	[32]
12	IMI685	Ti-6.18Al-5.27Zr-0.5Mo-0.28Si	685-βST1050 °C-WQ	550 °C-24 h	Lamellar α'—No precipitates	IMI685-2	[32]
13	IMI685	Ti-6.18Al-5.27Zr-0.5Mo-0.28Si	685-βST1050 °C-WQ	650 °C-24 h	Lamellar-Silicides S1 & S2—NO Ti_3Al	IMI685-3	[32]
14	IMI685	Ti-6.18Al-5.27Zr-0.5Mo-0.28Si	685-βST1050 °C-WQ	700 °C-24 h	Lamellar-Silicides S2—NO Ti_3Al	IMI685-4	[32]
15	IMI685	Ti-6.18Al-5.27Zr-0.5Mo-0.28Si	685-βST1050 °C-WQ	800 °C-24 h	Lamellar~0.1µm Silicides S2—NO Ti_3Al	IMI685-5	[32]
16	IMI685	Ti-6.18Al-5.27Zr-0.5Mo-0.28Si	685-βST1050 °C-WQ	700 °C-24 h	Lamellar-finer Silicides S2/41.2 nm—NO Ti_3Al	IMI685-6	[33]
17	IMI685	Ti-6.18Al-5.27Zr-0.5Mo-0.28Si	685-βST1050 °CWQ6CR	700 °C-24 h	Lamellar-finer Silicides S2/38.6 nm—NO Ti_3Al	IMI685-7	[33]
18	IMI685	Ti-6.18Al-5.27Zr-0.5Mo-0.28Si	685-βST1050 °CWQ12CR	700 °C-24 h	Lamellar-finer Silicides S2/33.4 nm—NO Ti_3Al	IMI685-8	[33]
19	IMI685	Ti-6.18Al-5.27Zr-0.5Mo-0.28Si	685-βST1050 °CWQ15CR	700 °C-24 h	Lamellar-finer Silicides S2/28.5 nm-NO Ti_3Al	IMI685-9	[33]

Table A1. *Cont.*

Sl#	*Alloy*	*Chemistry (Nominal)*	*Processing Step 1*	*Processing Step 2*	*Microstructure Description*	*Alloy Designation*	*Ref.*
20	IMI829	Ti-6.1Al-3.3Sn-3.2Zr-1Nb-0.5Mo-0.32Si	829-βST1050 °C-WQ	Unaged	Lamellar α'—No precipitates	IMI829-1	[34]
21	IMI829	Ti-6.1Al-3.3Sn-3.2Zr-1Nb-0.5Mo-0.32Si	829-βST1050 °C-WQ	625 °C-24 h	Lamellar—Silicides S2 only-No Ti_3Al	IMI829-2	
22	IMI829	Ti-6.1Al-3.3Sn-3.2Zr-1Nb-0.5Mo-0.32Si	829-βST1050 °C-OQ	Unaged	Lamellar α'—No precipitates	IMI829-3	
23	IMI829	Ti-6.1Al-3.3Sn-3.2Zr-1Nb-0.5Mo-0.32Si	829-βST1050 °C-OQ	625 °C-24 h	Lamellar-Silicides S2 only-No Ti_3Al	IMI829-4	
24	IMI829	Ti-6.1Al-3.3Sn-3.2Zr-1Nb-0.5Mo-0.32Si	829-βST1050 °C-AC	Unaged	Lamellar/Widmanstatten-No precipitates-No Silicides or Ti_3Al	IMI829-5	
25	IMI829	Ti-6.1Al-3.3Sn-3.2Zr-1Nb-0.5Mo-0.32Si	829-βST1050 °C-AC	625 °C-24 h	Lamellar/Widmanstatten-Silicides S2 only-No Ti_3Al	IMI829-6	
26	IMI829	Ti-6.1Al-3.3Sn-3.2Zr-1Nb-0.5Mo-0.32Si	829-βST1050 °C-FC	Unaged	Aligned alpha/Lamellar—No precipitates	IMI829-7	
27	IMI829	Ti-6.1Al-3.3Sn-3.2Zr-1Nb-0.5Mo-0.32Si	829-βST1050 °C-FC	625 °C-24 h	Aligned alpha/LamellarS2—Ti_3Al	IMI829-8	
28	IMI829	Ti-5.54Al-3.48Sn-2.95Zr-0.97Nb-0.34Mo-0.28Si	829-βST1050 °C-AC	Unaged	Lamellar- No pecipitates	IMI829-9	[35]
29	IMI829	Ti-5.54Al-3.48Sn-2.95Zr-0.97Nb-0.34Mo-0.28Si	829-βST1050 °C-AC	625 °C-2 h-AC-575 °C-1000 h-AC	Lamellar—Ti_3Al (5 nm)	IMI829-10	
30	IMI829	Ti-5.51Al-3.48Sn-3.04Zr-0.99Nb-0.33Mo < 0.02Si	829NS-βST1050 °C-AC	Unaged	Lamellar-No precipitates	IMI829NS-1	
31	IMI829	Ti-5.51Al-3.48Sn-3.04Zr-0.99Nb-0.33Mo < 0.02Si	829NS-βST1050 °C-AC	625 °C-2 h-AC-575 °C-1000 h-AC	Lamellar—Ti_3Al (5 nm)	IMI829NS-2	
32	Ti-1100	Ti-6Al-2.8Sn-4Zr-0.4Mo-0.45Si	Ti1100-βST1093 °C-AC	Unaged (593C-8 h-AC)	Lamellar-No precipitates	Ti-1100-8	[36]
33	Ti-1100	Ti-6Al-2.8Sn-4Zr-0.4Mo-0.45Si	Ti1100-βST1093 °C-AC	Overaged (Unaged + 593C-180 K min-AC)	Lamellar-13 nm Ti_3Al in Tr β and 175 × 35 nm Silicides	Ti-1100-9	
34	Ti-1100	Ti-6Al-2.8Sn-4Zr-0.4Mo-0.45Si	Ti1100-βST1093 °C-AC	PAHT (Unaged + 593C-60 K min + 750C-4 h-AC)	Lamellar-only Silicides (~100 nm)-NO Ti_3Al	Ti-1100-10	
35	IMI834	Ti-5.07Al-3.08Sn-3.45Zr-0.31Mo-0.2Si-0.66Nb-0.04C	834-βST1080 °C-cooled to (α + β)1010 °C-1 h-WQ	Unaged	Lamellar-No precipitates	IMI834-4	[37]
36	IMI834	Ti-5.07Al-3.08Sn-3.45Zr-0.31Mo-0.2Si-0.66Nb-0.04C	834-βST1080 °C-cooled to (α + β)1010 °C-1 h-WQ	700 °C-2 h-AC	Lamellar—Ti_3Al (5 nm) in Tr. β and Silicides	IMI834-5	
37	IMI834	Ti-5.07Al-3.08Sn-3.45Zr-0.31Mo-0.2Si-0.66Nb-0.04C	834-βST1080 °C-cooled to (α + β)1010 °C-1 h-WQ	825 °C-2 h-WQ	Lamellar—100 to 175 nm Silicides (Ti_3Al dissolved at 825 °C)	IMI834-6	

Table A1. *Cont.*

Sl#	Alloy	Chemistry (Nominal)	Processing Step 1	Processing Step 2	Microstructure Description	Alloy Designation	Ref.
38	IMI834	Ti-5.78Al-4.54Sn-4.05Zr-0.70Nb-0.52Mo-0.44Si-0.055C	834-(α + β)ST1020 °C-2 h-OQ (12-15%αp)	600 °C-4 h	Bimodal-Ti_3Al in only αp	IMI834-7	[38]
39	IMI834	Ti-5.78Al-4.54Sn-4.05Zr-0.70Nb-0.52Mo-0.44Si-0.055C	834-(α + β)ST1020 °C-2 h-OQ-(12-15%αp)	650 °C-4 h	Bimodal-Ti_3Al in αp & Tr. β and Silicides S2	IMI834-8	
40	IMI834	Ti-5.78Al-4.54Sn-4.05Zr-0.70Nb-0.52Mo-0.44Si-0.055C	834-(α + β)ST1020 °C-2 h-OQ-(12-15%αp)	700 °C-4 h	Bimodal-Ti_3Al in αp & Tr. β and Silicides S2	IMI834-9	
41	WJZ-Ti	Ti-6.7Al-1.9Sn-3.9Zr-4.6Mo-0.96W-0.23Si	834-(α + β)ST940 °C-2 h-AC	Unaged	Bimodal-No precipitates	WJZ-Ti-1	[39]
42	WJZ-Ti	Ti-6.7Al-1.9Sn-3.9Zr-4.6Mo-0.96W-0.23Si	834-(α + β)ST940 °C-1 h-AC	600 °C-2 h	Bimodal-6 nm Ti_3Al in αp	WJZ-Ti-2	
43	WJZ-Ti	Ti-6.7Al-1.9Sn-3.9Zr-4.6Mo-0.96W-0.23Si	834-(α + β)ST940 °C-1 h-AC	750 °C-2 h	Bimodal-7 nm Ti_3Al in αp & Tr.β	WJZ-Ti-3	
44	WJZ-Ti	Ti-6.7Al-1.9Sn-3.9Zr-4.6Mo-0.96W-0.23Si	834-(α + β)ST940 °C-1 h-AC	750 °C-12 h	Bimodal-15 nm Ti_3Al in αp & Tr.β	WJZ-Ti-4	
45	TA29	Ti-5.8Al-4Sn-4Zr-0.7Nb-1.5Ta-0.4Si-0.06C	TA29-βST (at > 1050 °C)	750 °C-2 h	Lamellar—~100 nm Silicides -small number at IPB	TA29-1	[40]
46	TA29	Ti-5.8Al-4Sn-4Zr-0.7Nb-1.5Ta-0.4Si-0.06C	TA29-βST (at > 1050 °C) + 750 °C-2 h	650 °C-8 h	Lamellar—~100 nm Silicides at IPB & Ti_3Al (<5 nm)	TA29-2	
77	TA29	Ti-5.8Al-4Sn-4Zr-0.7Nb-1.5Ta-0.4Si-0.06C	TA29-βST (at > 1050 °C) + 750 °C-2 h	650 °C-100 h	Lamellar—~100 nm-Silicides at IPB and some inside &Ti_3Al in Tr. β (~8 nm)	TA29-3	
48	TA29	Ti-5.8Al-4Sn-4Zr-0.7Nb-1.5Ta-0.4Si-0.06C	TA29-βST (at > 1050 °C) + 750 °C-2 h	650 °C-500 h	Lamellar—~100 nm Silicides at IPB and inside-IPB & Ti_3Al in Tr. β (26 nm L x13 nm thk.)	TA29-4	
49	TA29	Ti-5.8Al-4Sn-4Zr-0.7Nb-1.5Ta-0.4Si-0.06C	TA29-βST (at > 1050 °C) + 750 °C-2 h	650 °C-1000 h	Lamellar—~100 nm Silicides at IPB and inside & Ti_3Al in Tr. β (~20 nm dia.)	TA29-5	
50	KIMS	Ti-6.5Al-3Sn-4Hf-0.2Nb-0.4Mo-0.4Si-0.1B	KIMS-(α + β)ST-1 h-WQ	650 °C-5 h	Bimodal—Ti_3Al αp & Tr.β uniformly and Silicides-~80 nm	KIMS-1	[41]
51	KIMS	Ti-6.5Al-3Sn-4Hf-0.2Nb-0.4Mo-0.4Si-0.1B	KIMS-(α + β)ST-1 h-WQ	700 °C-2 h-AC	Bimodal—150 nm Silicides-IPB	KIMS-2	
52	JZ1	Ti-5.6Al-4.8Sn-2Zr-1Mo-0.35Si	JZ1-(α + β)ST-1005 °C-2 h-AC	700 °C-2 h-AC	Bimodal—No precipitates	JZ1-1	[42]
53	JZ1	Ti-5.6Al-4.8Sn-2Zr-1Mo-0.35Si	JZ1-(α + β)ST-1005 °C-2 h-AC	700 °C-5 h-AC	Bimodal—Ti_3Al in αp + Silicides (~100 nm)	JZ1-2	
54	JZ1	Ti-5.6Al-4.8Sn-2Zr-1Mo-0.35Si	JZ1-(α + β)ST-1005 °C-2 h-AC	700 °C-15 h-AC	Bimodal—Ti_3Al in αp + Silicides (~100 nm)	JZ1-3	
55	JZ1	Ti-5.6Al-4.8Sn-2Zr-1Mo-0.35Si	JZ1-(α + β)ST-1005 °C-2 h-AC	700 °C-2 h-AC-600 °C-100 h	Bimodal—Ti_3Al in αp + Silicides	JZ1-4	
56	JZ1	Ti-5.6Al-4.8Sn-2Zr-1Mo-0.35Si	JZ1-(α + β)ST-1005 °C-2 h-AC	700 °C-5h-AC-600 °C-100 h	Bimodal—Ti_3Al in αp + Silicides (~100 nm)	JZ1-5	
57	JZ1	Ti-5.6Al-4.8Sn-2Zr-1Mo-0.35Si	JZ1-(α + β)ST-1005 °C-2 h-AC	700 °C-15h-AC-600 °C-100 h	Bimodal—Ti_3Al in αp + Silicides (~100 nm)	JZ1-6	

Table A1. *Cont.*

Sl#	Alloy	Chemistry (Nominal)	Processing Step 1	Processing Step 2	Microstructure Description	Alloy Designation	Ref.
58	JZ2	Ti-6Al-4.8Sn-2Zr-1Mo-0.35Si	JZ2-(α + β)ST-1015 °C-2 h-AC	760 °C-2 h-AC	Bimodal—Ti_3Al in αp + Silicides	JZ2-1	
59	JZ2	Ti-6Al-4.8Sn-2Zr-1Mo-0.35Si	JZ2-(α + β)ST-1015 °C-2 h-AC	760 °C-5h-AC	Bimodal—Ti_3Al in αp + Silicides (~100 nm)	JZ2-2	
60	JZ2	Ti-6Al-4.8Sn-2Zr-1Mo-0.35Si	JZ2-(α + β)ST-1015 °C-2 h-AC	760 °C-10 h-AC	Bimodal—Ti_3Al in αp + Silicides	JZ2-3	
61	JZ2	Ti-6Al-4.8Sn-2Zr-1Mo-0.35Si	JZ2-(α + β)ST-1015 °C-2 h-AC	760 °C-2 h-AC	Bimodal—Ti_3Al in αp & Tr.β + Silicides	JZ2-4	
62	JZ2	Ti-6Al-4.8Sn-2Zr-1Mo-0.35Si	JZ2-(α + β)ST-1015 °C-2 h-AC	760 °C-5h-AC-600 °C-100 h	Bimodal—Ti_3Al in αp & Tr.β + Silicides (~100 nm)	JZ2-5	
63	JZ2	Ti-6Al-4.8Sn-2Zr-1Mo-0.35Si	JZ2-(α + β)ST-1015 °C-2 h-AC	760 °C-10 h-AC-600 °C-100 h	Bimodal—Ti_3Al in αp & Tr.β + Silicides	JZ2-6	
64	Ti60	Ti-5.8Al-4Sn-3.5Zr-0.4Mo-0.4Nb-1Ta-0.4Si-0.06C	TA60-(α + β)ST1010 °C-2 h-OQ	Unaged	Bimodal—No precipitates	Ti60-1	[43]
65	Ti60	Ti-5.8Al-4Sn-3.5Zr-0.4Mo-0.4Nb-1Ta-0.4Si-0.06C	TA60-(α + β)ST1010 °C-2 h-OQ	650 °C-2 h-AC	Bimodal-No Ti_3Al+ small number of Silicides 100 nm-Stage 1	Ti60-2	
66	Ti60	Ti-5.8Al-4Sn-3.5Zr-0.4Mo-0.4Nb-1Ta-0.4Si-0.06C	TA60-(α + β)ST1010 °C-2 h-OQ	650 °C-4 h-AC	Bimodal-No Ti_3Al+ small number of Silicides-100 nm-Stage 1	Ti60-3	
67	Ti60	Ti-5.8Al-4Sn-3.5Zr-0.4Mo-0.4Nb-1Ta-0.4Si-0.06C	TA60-(α + β)ST1010 °C-2 h-OQ	650 °C-8 h-AC	Bimodal-No Ti_3Al + Silicides—100 nm-Stage 1	Ti60-4	
68	Ti60	Ti-5.8Al-4Sn-3.5Zr-0.4Mo-0.4Nb-1Ta-0.4Si-0.06C	TA60-(α + β)ST1010 °C-2 h-OQ	650 °C-16 h-AC	Bimodal-No Ti_3Al + Silicides—100 nm —Stage 1	Ti60-5	
69	Ti60	Ti-5.8Al-4Sn-3.5Zr-0.4Mo-0.4Nb-1Ta-0.4Si-0.06C	TA60-(α + β)ST1010 °C-2 h-OQ	700 °C-2 h-AC	Bimodal-No Ti_3Al + Silicides 100 nm Stage 1	Ti60-6	
70	Ti60	Ti-5.8Al-4Sn-3.5Zr-0.4Mo-0.4Nb-1Ta-0.4Si-0.06C	TA60-(α + β)ST1010 °C-2 h-OQ	700 °C-4 h-AC	Bimodal-Ti_3Al in αp + Silicides	Ti60-7	
71	Ti60	Ti-5.8Al-4Sn-3.5Zr-0.4Mo-0.4Nb-1Ta-0.4Si-0.06C	TA60-(α + β)ST1010 °C-2 h-OQ	700 °C-8 h-AC	Bimodal-Ti_3Al in αp + Silicides	Ti60-8	
72	Ti60	Ti-5.8Al-4Sn-3.5Zr-0.4Mo-0.4Nb-1Ta-0.4Si-0.06C	TA60-(α + β)ST1010 °C-2 h-OQ	700 °C-16 h-AC	Bimodal-Ti_3Al in αp + Silicides	Ti60-9	
73	Ti60	Ti-5.8Al-4Sn-3.5Zr-0.4Mo-0.4Nb-1Ta-0.4Si-0.06C	TA60-(α + β)ST1010 °C-2 h-OQ	700 °C-24 h-AC	Bimodal-Ti_3Al in αp + Silicides	Ti60-10	
74	Ti60	Ti-5.8Al-4Sn-3.5Zr-0.4Mo-0.4Nb-1Ta-0.4Si-0.06C	TA60-(α + β)ST1010 °C-2 h-OQ	700 °C-48 h-AC	Bimodal-Ti_3Al in αp + Silicides	Ti60-11	
75	Ti60	Ti-5.8Al-4Sn-3.5Zr-0.4Mo-0.4Nb-1Ta-0.4Si-0.06C	TA60-(α + β)ST1010 °C-2 h-OQ	750 °C-2 h-AC	Bimodal-Silicides-Ti_3Al in αp	Ti60-12	
76	Ti60	Ti-5.8Al-4Sn-3.5Zr-0.4Mo-0.4Nb-1Ta-0.4Si-0.06C	TA60-(α + β)ST1010 °C-2 h-OQ	750 °C-4 h-AC	Bimodal-Ti_3Al in αp + Silicides	Ti60-13	

Table A1. *Cont.*

Sl#	*Alloy*	*Chemistry (Nominal)*	*Processing Step 1*	*Processing Step 2*	*Microstructure Description*	*Alloy Designation*	*Ref.*
77	Ti60	Ti-5.8Al-4Sn-3.5Zr-0.4Mo-0.4Nb-1Ta-0.4Si-0.06C	TA60-(α + β)ST1010 °C-2 h-OQ	750 °C-8 h-AC	Bimodal-Ti_3Al in αp + Silicides	Ti60-14	
78	Ti60	Ti-5.8Al-4Sn-3.5Zr-0.4Mo-0.4Nb-1Ta-0.4Si-0.06C	TA60-(α + β)ST1010 °C-2 h-OQ	750 °C-16 h-AC	Bimodal-Ti_3Al in αp + Silicides—100 nm	Ti60-15	
79	Ti60	Ti-5.8Al-4Sn-3.5Zr-0.4Mo-0.4Nb-1Ta-0.4Si-0.06C	TA60-1035C-near β forged-(α + β)ST1010 °C-2 h-AC	700 °C-2 h-AC	Bimodal-No Ti_3Al + Silicides-~100 nm	Ti60-16	[44]
80	Ti60	Ti-5.8Al-4Sn-3.5Zr-0.4Mo-0.4Nb-1Ta-0.4Si-0.06C	TA60-1035C-near β forged-(α + β) ST1010 °C-2 h-AC	700 °C-2 h-AC-600C-100 h-AC	Bimodal-Ti_3Al in αp + Silicides ~200 nm	Ti60-17	[44]
81	Ti60	Ti-5.8Al-4Sn-3.5Zr-0.4Mo-0.4Nb-1Ta-0.4Si-0.06C	TA60-1035C-near β forged-(α + β)ST1010 °C-2 h-AC	700 °C-2 h-A -700 °C-100 h-AC	Bimodal-only Silicides possibly (dissolution of Ti_3Al)	Ti60-18	[44]
82	Ti60	Ti-5.8Al-4Sn-3.5Zr-0.4Mo-0.4Nb-1Ta-0.4Si-0.06C	TA60-1035C-near β forged-(α + β)ST1010 °C-2 h-AC	700 °C-2 h-AC-750 °C-100 h-AC	Bimodal-only Silicides possibly (dissolution of Ti_3Al)	Ti60-19	[44]
83	Ti60	Ti-5.8Al-4Sn-3.5Zr-0.4Mo-0.4Nb-1Ta-0.4Si-0.06C	TA60-1070C- β forged-(α + β)ST1010 °C-2 h-AC	700 °C-2 h-AC	Lamellar + No Ti_3Al + Silicides ~100 nm	Ti60-20	[44]
84	Ti60	Ti-5.8Al-4Sn-3.5Zr-0.4Mo-0.4Nb-1Ta-0.4Si-0.06C	TA60-1070C-β forged-(α + β)ST1010 °C-2 h-AC	700 °C-2 h-AC-600 °C-100 h-AC	Lamellar-Ti_3Al in Tr. β + Silicides ~100 nm	Ti60-21	[44]
85	JL	Ti-5.6Al-4.3Sn-3Zr-1Mo-0.8Nd-0.34Si	JL-(α + β) forged-(α + β)ST1010 °C-2 h-AC	Unaged	Bimodal—No precipitates (αp is ~10% vf.;~150 nm)	JL-1	[45]
86	JL	Ti-5.6Al-4.3Sn-3Zr-1Mo-0.8Nd-0.34Si	JL-(α + β) forged-(α + β)ST1010 °C-2 h-AC	700 °C-2 h-AC	Bimodal—Ti_3Al in αp + Silicides ~125 nm	JL-2	[45]
87	JL	Ti-5.6Al-4.3Sn-3Zr-1Mo-0.8Nd-0.34Si	JL-(α + β) forged-(α + β)ST1010 °C-2 h-AC	700 °C-12 h-AC	Bimodal—Ti_3Al in αp & Tr. β + Silicides ~125 nm	JL-3	[45]
88	JL	Ti-5.6Al-4.3Sn-3Zr-1Mo-0.8Nd-0.34Si	JL-(α + β) forged-βST1030 °C-2 h-AC	Unaged	Lamellar—No precipitates (colony size; ~350 nm)	JL-4	[45]
89	JL	Ti-5.6Al-4.3Sn-3Zr-1Mo-0.8Nd-0.34Si	JL-(α + β) forged-βST1030 °C-2 h-AC	700 °C-2 h-AC	Lamellar—Ti_3Al in Tr. β + Silicides ~125 nm	JL-5	[45]
90	JL	Ti-5.6Al-4.3Sn-3Zr-1Mo-0.8Nd-0.34Si	JL-(α + β) forged-βST1030 °C-2 h-AC	700 °C-12 h-AC	Lamellar—Ti_3Al in Tr. β + Silicides ~125 nm	JL-6	[45]
91	IMI834	Ti-5.8Al-4Sn-3.5Zr-0.7Mo-0.35Si-0.7Nb-0.06C	834-(α + β) ST1020 °C-2 h-AC	700 °C-2 h-AC	Bimodal—Ti_3Al in αp + Silicides ~125 nm	IMI834-10	[46]

Table A1. *Cont.*

Sl#	*Alloy*	*Chemistry (Nominal)*	*Processing Step 1*	*Processing Step 2*	*Microstructure Description*	*Alloy Designation*	*Ref.*
92	Ti6242S	Ti-5.7Al-1.9Sn-3.7Zr-1.9Mo-0.09Si	Ti6242S-(α + β) Hot rolled βST1052 °C-1 h-CC	Unaged	Lamellar-No precipitates	Ti6242-1	[47]
93	Ti6242S	Ti-5.7Al-1.9Sn-3.7Zr-1.9Mo-0.09Si	Ti6242S-(α + β) Hot rolled β ST1052 °C-1 h-CC	760 °C-600 h-AC	Lamellar-Silicides (>100 nm)	Ti6242-2	
94	LD-Ti423	Ti-8Al-1Cr-1V-0.5Fe-0.1Si	VIM-Open die forged at (β)1100 °C-Hot rolled at (α + β)1000 °C-50%Reduction (Rolled plate) or HR	NA	Heterogenous microstructure/similar to bimodal (major equiaxed α_p 11 µm and small amount of acicular αs and β phases in the interstices of equiaxed α)	LD-Ti423-1	[48]
95	LD-Ti423	Ti-8Al-1Cr-1V-0.5Fe-0.1Si	VIM-Open die forged at (β)1100 °C-Hot rolled at (α + β)1000 °C-50%Reduction (Rolled plate)	HR +(α + β) ST at 1000 °C-1 h-AC-Aged at 560 °C-4 h-AC (STA)	Heterogenous microstructure/similar to bimodal (major equiaxed α_p 20µm and small amount of acicular αs and β phases in the interstices of equiaxed α)	LD-Ti423-2	
96	TMC-Ti213	Ti-2Al-1.3V	Thermomechanical consolidation (TMC) of TiH_2 and Ti6Al4V at a mass ratio of 2:1, and extruded to produce Ti-2Al-1.3V at 16 to 1 ratio at around 1200 °C	TMC-Vac Anneal 700 °C-6 h-FC	lamellar α/β (lamellae of 0.9µm thk and ave. lamellar colony size of 15.4 µm)	TMC-Ti213-1	[49]
97	TMC-Ti213	Ti-2Al-1.3V	Thermomechanical consolidation (TMC) of TiH_2 and Ti6Al4V at a mass ratio of 2:1, and extruded to produce Ti-2Al-1.3V at 16 to 1 ratio at around 1200 °C	TMC-Vac Anneal 700 °C-6 h-FC-980 °C-1 h-AC	equiaxed α grains and α/β lamellar structured domains (βt or β transformed structure)	TMC-Ti213-2	
98	TA19	Ti-6.6Al-1.75Sn-4.12Zr-1.91Mo-0.32W-0.1Si	α-β field rolled plate, tempered in the α-β field	970 °C-1 h-AC (for equiaxed structure (EM))	equiaxed α grains (42%Vol.; 12 µm dia) and α/β lamellar (αs 10 µm length × 400 nm width); g.b α 420 nm width	TA19-1	[50]
99	TA19	Ti-6.6Al-1.75Sn-4.12Zr-1.91Mo-0.32W-0.1Si	α-β field rolled plate, tempered in the α-β field	1015 °C-35s-cooled at 20 °C/s (for semi equiaxed structure (S-EM))	Semi-equiaxed α grains (41%Vol.; 13 µm dia) and α/β lamellar (αs 11 µm length × 410 nm width); g.b α 850 nm width	TA19-2	

Table A1. *Cont.*

Sl#	*Alloy*	*Chemistry (Nominal)*	*Processing Step 1*	*Processing Step 2*	*Microstructure Description*	*Alloy Designation*	*Ref.*
100	TKT-1	Ti-4.8Al-2.3Sn-4.2Zr-2Mo	Double melted; β forged qt 1100 °C-groove rolled to 50% reduction at (α + β) 960 °C to rods of 14mm dia	Annealed at 950 °C-1 h-AC-aged at 590 °C-8 h-AC	Bimodal microstructure comprising primary equiaxed α and α-β lamellar (transformed β) structures	TKT-1	[51]
101	TKT-2	Ti-4.8Al-2.2Sn-4.1Zr-2Mo-1.1Ge	Double melted; β forged qt 1100 °C-groove rolled to 50% reduction at (α + β) 960 °C to rods of 14mm dia	Annealed at 950 °C-1 h-AC-aged at 590 °C-8 h-AC	Bimodal microstructure comprising primary equiaxed α and α-β lamellar (transformed β) structures	TKT-2	
102	TKT-6	Ti-4.9Al-2.3Sn-4.1Zr-2.1Mo-0.1Si-0.8Ge	Double melted; β forged qt 1100 °C-groove rolled to 50% reduction at (α + β) 960 °C to rods of 14mm dia	Annealed at 950 °C-1 h-AC-aged at 590 °C-8 h-AC	Bimodal microstructure comprising primary equiaxed α and α-β lamellar (transformed β) structures with $(TiZr)_6(SiGe)_3$ precipitates	TKT-6	
103	PC	Ti-6Al-3.5Sn-4.5Zr-2.0Ta-0.7Nb-0.5Mo-0.4Si	Induction skull melted ingot 80mm dia × 120mm length and then 1100 °C β upset forged to a total height reduction of 75% (reduction ratio of 4 to 1)	ONE-Isothermal Multidirectional Forging (IMDF) at 1020 °C-annealed at 650 °C-6 h	Mainly α laths (lamellar mainly—mean size 2.13 µm) with small amount of equiaxed α	PC-IMDF1	[52]
104	PC	Ti-6Al-3.5Sn-4.5Zr-2.0Ta-0.7Nb-0.5Mo-0.4Si	Induction skull melted ingot 80 mm dia × 120 mm length and then 1100C β upset forged to a total height reduction of 75% (reduction ratio of 4 to 1)	TWO-IMDFs at 1020 °C-annealed at 650 °C-6 h	prior β boundaries start to disappear and α laths transform to spheroidal α grains (equiaxed α—mean size 1.85 µm)	PC-IMDF2	
105	PC	Ti-6Al-3.5Sn-4.5Zr-2.0Ta-0.7Nb-0.5Mo-0.4Si	Induction skull melted ingot 80 mm dia × 120 mm length and then 1100 °C β upset forged to a total height reduction of 75% (reduction ratio of 4 to 1)	FOUR-IMDFs at 1020 °C-annealed at 650 °C-6 h	large number of spheroidal α grains transformed from lamellae	PC-IMDF4	

Note: ST: solution treated; h: hours; AC: air cooled; OQ: oil quenched; WQ: water quenched; α_p: primary alpha; Tr. β: transformed beta; bimodal matrix: primary α + transformed β; and lamellar matrix: completely transformed β.

Table A2. Database of 105 variants of 19 distinct near-α Ti alloys identified from the literature, which form the decision matrix comprising the alternatives and their attributes.

Alloy Desig.	*Grade*	*Al.eq.*	*Matrix*	*Precipitates*	*Size*	*YS*	*UTS*	*%El*	*Ref.*
IMI834-1	IMI834	8	Bimodal	NA	NA	1040	1125	9	[31]
IMI834-2	IMI834	8	Bimodal	NA	NA	1200	1255	13	
IMI834-3	IMI834	8	Lamellar	NA	NA	1110	1220	4	
Ti-1100-1	Ti-1100	7	Bimodal	NA	NA	900	965	13.5	
Ti-1100-2	Ti-1100	7	Bimodal	NA	NA	965	1050	14	
Ti-1100-3	Ti-1100	7	Bimodal	NA	NA	995	1090	8	
Ti-1100-4	Ti-1100	7	Lamellar	NA	NA	1050	1160	7.5	
Ti-1100-5	Ti-1100	7	Lamellar	NA	NA	1080	1190	5	
Ti-1100-6	Ti-1100	7	Bimodal	NA	NA	1100	1200	10	
Ti-1100-7	Ti-1100	7	Lamellar	NA	NA	1150	1250	2.5	
IMI685-1	IMI685	7	Lamellar	NP	0	919	1058	7.2	[32]
IMI685-2	IMI685	7	Lamellar	NP	0	966	1090	7.3	
IMI685-3	IMI685	7	Lamellar	Silicides	>50	1020	1132	4.7	
IMI685-4	IMI685	7	Lamellar	Silicides	>50	1005	1102	4.8	
IMI685-5	IMI685	7	Lamellar	Silicides	>50	954	1038	3.75	
IMI685-6	IMI685	7	Lamellar	Silicides	21–50	917.5	1021	5.55	[33]
IMI685-7	IMI685	7	Lamellar	Silicides	21–50	980	1064	4.9	
IMI685-8	IMI685	7	Lamellar	Silicides	21–50	978	1060	2.5	
IMI685-9	IMI685	7	Lamellar	Silicides	21–50	1025.5	1067	2.65	
IMI829-1	IMI829	8	Lamellar	NP	0	886	970	10	[34]
IMI829-2	IMI829	8	Lamellar	Silicides	>50	1005	1023	2	
IMI829-3	IMI829	8	Lamellar	NP	0	863	951	11	
IMI829-4	IMI829	8	Lamellar	Silicides	>50	960	1005	3	
IMI829-5	IMI829	8	Lamellar	NP	0	867	942	10	
IMI829-6	IMI829	8	Lamellar	Silicides	>50	858	975	7	
IMI829-7	IMI829	8	Lamellar	NP	0	866	946	9	
IMI829-8	IMI829	8	Lamellar	Silicides	>50	851	953	6.5	
IMI829-9	IMI829	7	Lamellar	NP	0	861	977.5	9.6	[35]
IMI829-10	IMI829	7	Lamellar	Silicides aided by Ti_3Al in Tr.β	>50	881.5	953	3.1	
IMI829NS-1	IMI829	7	Lamellar	NP	0	800	904	9.4	
IMI829NS-2	IMI829	7	Lamellar	Ti_3Al in Tr.β-3	<7	819.5	891.5	9.05	
Ti-1100-8	Ti-1100	8	Lamellar	NP	0	915	1000	5.5	[36]
Ti-1100-9	Ti-1100	8	Lamellar	Ti_3Al in Tr.β aided by Silicides	7–20	955	982	0.18	
Ti-1100-10	Ti-1100	8	Lamellar	Silicides	>50	895	980	4.15	
IMI834-4	IMI834	7	Lamellar	NP	0	987	1128	7.5	[37]
IMI834-5	IMI834	7	Lamellar	Ti_3Al in Tr.β-3	<7	1028	1134	6.5	
IMI834-6	IMI834	7	Lamellar	Silicides	>50	980	1098	7.5	

Table A2. *Cont.*

Alloy Desig.	*Grade*	*Al.eq.*	*Matrix*	*Precipitates*	*Size*	*YS*	*UTS*	*%El*	*Ref.*
IMI834-7	IMI834	8	Bimodal	Ti_3Al in αp-1	<7	905	1037	13	[38]
IMI834-8	IMI834	8	Bimodal	Ti_3Al in αp & Tr.β-2	7–20	953	1075	9.5	
IMI834-9	IMI834	8	Bimodal	Ti_3Al in αp & Tr.β-2	7–20	933	1060	8.7	
WJZ-Ti-1	WJZ-Ti	8	Bimodal	NP	0	1195	1300	18	[39]
WJZ-Ti-2	WJZ-Ti	8	Bimodal	Ti_3Al in αp-1	<7	1325	1450	18	
WJZ-Ti-3	WJZ-Ti	8	Bimodal	Ti_3Al in αp & Tr.β-2	7–20	1230	1250	12	
WJZ-Ti-4	WJZ-Ti	8	Bimodal	Ti_3Al in αp & Tr.β-2	7–20	1100	1120	5	
TA29-1	TA29	8	Lamellar	Silicides	>50	995	1062	7.5	[40]
TA29-2	TA29	8	Lamellar	Ti_3Al in Tr.β-3	<7	990	1075	6.5	
TA29-3	TA29	8	Lamellar	Ti_3Al in Tr.β-3	7–20	975	1060	3	
TA29-4	TA29	8	Lamellar	Ti_3Al in Tr.β-3	7–20	1018	1085	2.5	
TA29-5	TA29	8	Lamellar	Ti_3Al in Tr.β-3	7–20	975	1060	3.5	
KIMS-1	KIMS	8	Bimodal	Ti_3Al in αp & Tr.β-2	7–20	1113.8	1133.9	4.07	[41]
KIMS-2	KIMS	8	Bimodal	Silicides	>50	1032.6	1124.6	16.94	
JZ1-1	JZ1	8	Bimodal	NP	0	965	1030	15.5	[42]
JZ1-2	JZ1	8	Bimodal	Ti_3Al in αp-1	<7	965	1040	15	
JZ1-3	JZ1	8	Bimodal	Ti_3Al in αp-1	<7	940	1030	15	
JZ1-4	JZ1	8	Bimodal	Ti_3Al in αp-1	<7	1000	1060	16	
JZ1-5	JZ1	8	Bimodal	Ti_3Al in αp-1	<7	1000	1070	14.5	
JZ1-6	JZ1	8	Bimodal	Ti_3Al in αp-1	7-20	990	1060	15	
JZ2-1	JZ2	8	Bimodal	Ti_3Al in αp-1	<7	965	1060	15.5	
JZ2-2	JZ2	8	Bimodal	Ti_3Al in αp-1	7–20	960	1060	16.5	
JZ2-3	JZ2	8	Bimodal	Ti_3Al in αp-1	7–20	960	1050	17	
JZ2-4	JZ2	8	Bimodal	Ti_3Al in αp & Tr.β-2	7–20	1040	1110	14	
JZ2-5	JZ2	8	Bimodal	Ti_3Al in αp & Tr.β-2	7–20	1040	1110	12.5	
JZ2-6	JZ2	8	Bimodal	Ti_3Al in αp & Tr.β-2	7–20	1030	1100	13	
Ti60-1	Ti60	8	Bimodal	NP	0	960	1080	11	[43]
Ti60-2	Ti60	8	Bimodal	Silicides	>50	962	1082	10	
Ti60-3	Ti60	8	Bimodal	Silicides	>50	1000	1100	10	
Ti60-4	Ti60	8	Bimodal	Silicides	>50	1000	1100	9	
Ti60-5	Ti60	8	Bimodal	Silicides	>50	1000	1100	9	
Ti60-6	Ti60	8	Bimodal	Silicides	>50	982	1082	10	
Ti60-7	Ti60	8	Bimodal	Ti_3Al in αp-1	<7	970	1060	10	
Ti60-8	Ti60	8	Bimodal	Ti_3Al in αp-1	<7	960	1070	10	
Ti60-9	Ti60	8	Bimodal	Ti_3Al in αp-1	7–20	940	1060	10	

Table A2. *Cont.*

Alloy Desig.	*Grade*	*Al.eq.*	*Matrix*	*Precipitates*	*Size*	*YS*	*UTS*	*%El*	*Ref.*
Ti60-10	Ti60	8	Bimodal	Ti_3Al in αp-1	7–20	960	1080	10	
Ti60-11	Ti60	8	Bimodal	Ti_3Al in αp-1	7–20	980	1085	10	
Ti60-12	Ti60	8	Bimodal	Ti_3Al in αp-1	<7	960	1082	10	
Ti60-13	Ti60	8	Bimodal	Ti_3Al in αp-1	7–20	970	1080	9	
Ti60-14	Ti60	8	Bimodal	Ti_3Al in αp-1	7–20	965	1080	10	
Ti60-15	Ti60	8	Bimodal	Ti_3Al in αp-1	7–20	955	1077	11.5	
Ti60-16	Ti60	8	Bimodal	Silicides	>50	1010	1060	11	
Ti60-17	Ti60	8	Bimodal	Ti_3Al in αp-1	7–20	1050	1120	7	
Ti60-18	Ti60	8	Bimodal	Silicides	>50	1021	1090	12	[44]
Ti60-19	Ti60	8	Bimodal	Silicides	>50	950	1018	11.5	
Ti60-20	Ti60	8	Lamellar	Silicides	>50	1020	1080	9	
Ti60-21	Ti60	8	Lamellar	Ti_3Al in Tr.β-3	7–20	1040	1100	4	
JL-1	JL	8	Bimodal	NP	0	944	1029	15.6	
JL-2	JL	8	Bimodal	Ti_3Al in αp-1	<7	985	1057	12.2	
JL-3	JL	8	Bimodal	Ti_3Al in αp & Tr.β-2	<7	994	1066	12	[45]
JL-4	JL	8	Lamellar	NP	0	933	1020	12.4	
JL-5	JL	8	Lamellar	Ti_3Al in Tr.β-3	7–20	981	1052	8.4	
JL-6	JL	8	Lamellar	Ti_3Al in Tr.β-3	7–20	970	1042	6.5	
IMI834-10	IMI834	8	Bimodal	Ti_3Al in αp-1	<7	945	1012	14.5	[46]
Ti6242-1	Ti6242S	7	Lamellar	NP	0	837	946	12	[47]
Ti6242-2	Ti6242S	7	Lamellar	Silicides	>50	875	925	5.8	
LD-Ti423-1	LD-Ti423	8	Bimodal	NP	0	948	1046	8.3	[48]
LD-Ti423-2	LD-Ti423	8	Bimodal	NP	0	923	1013	8	
TMC-Ti213-1	TMC-Ti213	2	Lamellar	NP	0	996	1059	13.9	[49]
TMC-Ti213-2	TMC-Ti213	2	Bimodal	NP	0	876	994	7.4	
TA19-1	TA19	8	Bimodal	NP	0	984	1067	23.9	[50]
TA19-2	TA19	8	Bimodal	NP	0	1022	1113	22.8	
TKT-1	TKT-1	6	Bimodal	NP	0	980	1175	20	
TKT-2	TKT-2	6	Bimodal	NP	0	1075	1285	19	[51]
TKT-6	TKT-6	6	Bimodal	Germanides	<500	1060	1255	18	
PC-IMDF1	PC	8	Lamellar	NA	NA	982	1020	10.6	
PC-IMDF2	PC	8	Bimodal	NA	NA	1004	1043	12.7	[52]
PC-IMDF4	PC	8	Bimodal	NA	NA	1072	1118	15.6	

Note: NA: not available; NP: no precipitates.

References

1. Ikpe, E.; Ikechukwu, O.; Ebunilo, P.O.; Ikpe, E. Material selection for high pressure (HP) compressor blade for an aircraft engine. *Int. J. Adv. Mater. Res.* **2016**, *2*, 59–65.
2. Foltz, J.; Gram, M. Introduction to titanium and its alloys. In *ASM Handbook, Heat Treating of Nonferrous Alloys, Volume 4E*; Totten, G.E., MacKenzie, D.S., Eds.; ASM International: Materials Park, OH, USA, 2016.

3. Canumalla, R. On the low tensile ductility at room temperature in high temperature titanium alloys. *SCIREA J. Metall. Eng.* **2020**, *4*, 16–51.
4. Williams, J.C.; Boyer, R.R. Opportunities and issues in the application of titanium alloys for aerospace components. *Metals* **2020**, *10*, 705. [CrossRef]
5. Rao, M.N. Materials for gas turbines—An overview. In *Advances in Gas Turbine Technology*; Intechopen: Rijeka, Croatia, 2011; pp. 293–314.
6. Gogia, K. High-temperature titanium alloys. *Def. Sci. J.* **2005**, *55*, 149–173. [CrossRef]
7. Singh, K.; Ramachandra, C. Characterization of silicides in high temperature titanium alloys. *J. Mater. Sci.* **1997**, *32*, 229–234. [CrossRef]
8. Ramachandra, C.; Singh, V.; Rao, P.R. On silicides in high temperature Ti alloys. *Def. Sci. J.* **1986**, *36*, 207–220. [CrossRef]
9. Zhang, T.; Liu, C.-T. Design of titanium alloys by additive manufacturing: A critical review. *Adv. Powder Mater.* **2022**, *1*, 100014. [CrossRef]
10. Tshephe, S.T.; Akinwamide, S.O.; Olevsky, E.; Olubambi, P.A. Additive manufacturing of titanium-based alloys—A review of methods, properties, challenges, and prospects. *Heliyon* **2022**, *8*, e09041. [CrossRef]
11. *TIMETAL 834 Datasheet*; Titanium Metals Corporation: Warrensville Heights, OH, USA, 2000.
12. *TIMETAL 1100 Datasheet*; Titanium Metals Corporation: Warrensville Heights, OH, USA, 2008.
13. Ashby, M.F. *Materials and the Environment Eco-Informed Material Choice*, 1st ed.; Elsevier: Amsterdam, The Netherlands, 2009.
14. Ashby, M.F. *Materials Selection in Mechanical Design*, 5th ed.; Elsevier: Amsterdam, The Netherlands, 2017.
15. Jahan, A.; Ismail, M.Y.; Sapuan, S.M.; Mustapha, F. Materials screening and choosing methods—A review. *Mater. Des.* **2010**, *31*, 696–705. [CrossRef]
16. Anojkumar, L.; Ilangkumaran, M.; Sasirekha, V. Comparative analysis of MCDM methods for pipe material selectionin sugar industry. *Expert Syst. Appl.* **2014**, *41*, 2964–2980. [CrossRef]
17. Zhou, C.; Yin, G.F.; Hu, X.B. Multi-objective optimization of material selection for sustainable products: Artificial neural networks and genetic algorithm approach. *Mater. Des.* **2009**, *30*, 1209–1215. [CrossRef]
18. Rao, R.V.; Davim, J.P. A decision-making framework model for material selection using a combined multiple attribute decision-making method. *Int. J. Adv. Manuf. Technol.* **2008**, *35*, 751–760. [CrossRef]
19. Gupta, N. Material selection for thin-film solar cells using multiple attribute decision making approach. *Mater. Des.* **2011**, *32*, 1667–1671. [CrossRef]
20. Shanian, A.; Savadogo, O. A material selection model based on the concept of multiple attribute decision making. *Mater. Des.* **2006**, *27*, 329–337. [CrossRef]
21. Chauhan, A.; Vaish, R. Magnetic material selection using multiple attribute decision making approach. *Mater. Des.* **2012**, *36*, 1–5. [CrossRef]
22. Tzeng, G.H.; Huang, J.J. *Multiple Attribute Decision Making Methods and Applications*; CRC Press: Boca Raton, FL, USA, 2011.
23. Rao, R.V. *Decision Making in the Manufacturing Environment, Using Graph Theory and Fuzzy Multiple Attribute Decision Making Methods*; Springer: Berlin/Heidelberg, Germany, 2007.
24. Farag, M.M. *Materials and Process Selection in Engineering*; Elsevier Science and Technology: Amsterdam, The Netherlands, 1979.
25. Cherian, R.P.; Smith, L.N.; Midha, P.S. A neural network approach for selection for powder metallurgy materials and process parameters. *Artif. Intell. Eng.* **2000**, *14*, 39–44. [CrossRef]
26. Perez-Benitez, J.A.; Padovese, L.R. Feature Selection and Neural Network for analysis of microstructural changesin magnetic materials. *Expert Syst. Appl.* **2011**, *38*, 10547–10553. [CrossRef]
27. Zavadskas, K.; Turskis, Z.; Kildiene, S. State of art surveys of overviews on MCDM/MADM methods. *Technol. Econ. Dev. Econ.* **2014**, *20*, 165–179. [CrossRef]
28. Rajan, K. Materials Informatics. *Mater. Today* **2005**, *8*, 38–45. [CrossRef]
29. Cadima, J.; Jolliffle, I.T. Principal Component Analysis: A review and recent developments. *Phil. Trans. R. Soc. A* **2016**, *374*, 20150202.
30. George, L.; Hrubiak, R.; Rajan, K.; Saxena, S.K. Principal component analysis on properties of binary and ternary hydrides and a comparison of metal versus metal hydride properties. *J. Alloys Compd.* **2009**, *478*, 731–735. [CrossRef]
31. Peters, M.; Lee, Y.T.; Grundhoff, K.J.; Schurmann, H.; Welsch, G. Influence of processing on microstructure and mechanical properties of Ti-1100 and IMI 834. In Proceedings of the Minerals and Metals Society Fall Meeting, Detroit, MI, USA, 7–11 October 1991; pp. 533–548.
32. Ramachandra, C.; Singh, V. Effect of silicides on tensile properties and fracture of alloy Ti-6Al-5Zr-0.5Mo-0.25Si from 300 to 823 K. *J. Mater. Sci.* **1988**, *23*, 835–841. [CrossRef]
33. Ramachandra, C.; Singh, V. Effect of thermomechanical treatments on size and distribution of silicides and tensile properties of alloy Ti-6AI-5Zr-0.5Mo-0.25Si. *Metall. Trans. A* **1988**, *19*, 389–391. [CrossRef]
34. Sridhar, G.; Sarma, D.S. Structure and properties of a near-alpha titanium alloy after beta solution treatment and aging at 625 °C. *Metall. Trans. A* **1988**, *19*, 3025–3033. [CrossRef]
35. Woodfield, P.; Postans, P.J.; Loretto, M.; Smallman, R. The effect of long-term high temperature exposure on the structure and properties of the titanium alloy Ti-5331S. *Acta Metall.* **1988**, *36*, 507–515. [CrossRef]

36. Madsen, A.; Ghonem, H. Separating the effects of T3Al and silicide precipitates on the tensile and crack growth behavior at room temperature and 593 °C in a near-alpha titanium alloy. *J. Mater. Eng. Perform.* **1995**, *4*, 301–307. [CrossRef]
37. Srinadh, K.V.S.; Nidhi, S.; Singh, V. Role of Ti3Al/Silicides on tensile properties of Timetal 834 at various temperatures. *Bull. Mater. Sci.* **2007**, *30*, 595–600. [CrossRef]
38. Cope, M.T.; Hill, M.J. The influence of aging temperature on the mechanical properties of IMI 834. In Proceedings of the 6th World Conference on Titanium, Cannes, France, 6–9 June 1988.
39. Zhang, W.J.; Song, X.Y.; Hui, S.X.; Ye, W.J.; Yu, Y.; Li, Y.F. $\alpha 2$ phase precipitation behavior and tensile properties at room temperature and 650 °C in an ($\alpha + \beta$) titanium alloy. *Rare Met.* **2019**, *40*, 3261–3268. [CrossRef]
40. Li, J.; Cai, J.; Xu, Y.; Xiao, W.; Huang, X.; Ma, C. Influences of thermal exposure on the microstructural evolution and subsequent mechanical properties of a near-α high temperature titanium alloy. *Mater. Sci. Eng. A* **2020**, *774*, 138934. [CrossRef]
41. Narayana, P.; Kim, S.W.; Hong, J.K.; Reddy, N.; Yeom, J.T. Tensile properties of a newly developed high-temperature titanium alloy at room temperature and 650 °C. *Mater. Sci. Eng.* **2018**, *718*, 287–291. [CrossRef]
42. Zhang, J.; Peng, N.; Wang, Q.; Wang, X. A new aging treatment way for near α high temperature titanium alloys. *J. Mater. Sci. Technol.* **2009**, *25*, 454–458.
43. Jia, W.; Zeng, W.; Yu, H. Effect of aging on the tensile properties and microstructures of a near-alpha titanium alloy. *Mater. Des.* **2014**, *58*, 108–115. [CrossRef]
44. Jia, W.; Zeng, W.; Liu, J.; Zhou, Y.; Wang, Q. Influence of thermal exposure on the tensile properties and microstructures of Ti60 titanium alloy. *Mater. Sci. Eng. A* **2011**, *2011*, 511–518. [CrossRef]
45. Liu, J.; Li, S.; Li, D.; Yang, R. Effect of aging on fatigue-crack growth behavior of a high temperature titanium alloy. *Mater. Trans.* **2004**, *5*, 1577–1585. [CrossRef]
46. Singh, N.; Gauthama; Singh, V. Low cycle fatigue behavior of Ti alloy IMI 834 at room temperature. *Mater. Sci. Eng. A* **2002**, *325*, 324–332. [CrossRef]
47. Allison, J.E.; Cho, W.; Jones, J.W.; Donlon, W.T.; Lasecki, J.V. The influence of elevated temperature on the mechanical behavior of alpha/beta titanium alloys. In Proceedings of the Sixth World Conference on Titanium, Cannes, France, 6–9 June 1988.
48. Zhu, S.; Zhu, C.; Luo, D.; Zhang, X.; Zhou, K. Development of a Low-Density and High-Strength Titanium Alloy. *Metals* **2023**, *13*, 251. [CrossRef]
49. Zhang, Y.; Wu, X.; Zhang, B.; Zhang, Y.; Zhang, D. Microstructure and mechanical properties of a novel PM Ti–2Al–1.3V alloy in different heat treatment conditions. *Heat Treat. Surf. Eng.* **2022**, *4*, 43–53. [CrossRef]
50. Luo, M.; Lin, T.; Zhou, L.; Li, W.; Liang, Y.; Han, M.; Liang, Y. Deformation Behavior and Tensile Properties of the Semi-Equiaxed Microstructure in Near Alpha Titanium Alloy. *Materials* **2021**, *14*, 3380. [CrossRef]
51. Kitashima, T.; Suresh, K.S.; Yamba-Mitarai, Y. Effect of germanium and silicon additions on the mechanical properties of a near-α titanium alloy. *Mater. Sci. Eng. A* **2014**, *597*, 212–218. [CrossRef]
52. Zhang, J.; Guo, C.X.; Zhang, S.Z.; Feng, H.; Chen, C.Y.; Zhang, H.Z.; Cao, P. Microstructural manipulation and improved mechanical properties of a near α titanium alloy. *Mater. Sci. Eng. A* **2020**, *771*, 138569. [CrossRef]
53. Jahan, A.; Edwards, K.L.; Bahraminasab, M. *Multi-Criteria Decision Analysis—For Supporting the Selection of Engineering Materials in Product Design*, 2nd ed.; Elsevier: Amsterdam, The Netherlands, 2016.
54. Memariani, A.; Amini, A.; Alinezhad, A. Sensitivity analysis of simple additive weighting method (SAW): The results of change in the weight of one attribute on the final ranking alternatives. *J. Ind. Eng.* **2009**, *4*, 13–18.
55. Afshari, A.; Mojaahed, M.; Yusuff, R.M. Simple additive weighting approach to personal selection problem. *Int. J. Innov. Mgt. Technol.* **2010**, *1*, 511–515.
56. Madic, M.; Radovanovic, M.; Manic, M. Application of the ROV method of selection of cutting fluids. *Decis. Sci. Lett.* **2016**, *5*, 245–254. [CrossRef]
57. Jha, G.K.; Chatterjee, P.; Chatterjee, R.; Chakraborty, S. Suppliers selection in a manufacturing environment using a range of value method. *J. Mech. Eng.* **2013**, *3*, 16–22. [CrossRef]
58. Zavadskas, K.; Turskis, Z.; Vilutiene, T. Multiple criteria analysis of foundation installment alternatives by applying additive ratio assessment (ARAS) method. *Arch. Civil Mech. Eng.* **2010**, *10*, 123–141. [CrossRef]
59. Zavadskas, K.; Turskis, Z. A new additive ratio assessment (ARAS) method in multicriterial decision making. *Technol. Econ. Dev. Econ.* **2010**, *16*, 159–172. [CrossRef]
60. Stanujic, S.; Jovanovic, R. Measuring a quality of faculty website using ARAS method. *Contemp. Issues Bus. Manag. Educ.* **2012**, *2012*, 545–554.
61. Yazdabi, M.; Zavadskas, E.K.; Turskis, Z. A combined compromise solution (CoCoSo) method for multi-criteria decision-making problems. *Manag. Desicion* **2019**, *57*, 2501–2519.
62. Qiyas, M.; Naeem, M.; Khan, S.; Abdullah, S.; Botmart, T.; Shah, T. Decision support system based on CoCoSo method with the picture fuzzy information. *J. Math.* **2022**, *2022*, 1476233. [CrossRef]
63. Mefgouda, B.; Idoudi, H. A novel MADM based netwrok interface selection approach with rank reversal avoidance in HWNs. In Proceedings of the 2022 IEEE Wireless Communications and Networking Conference, Austin, TX, USA, 10–13 April 2022.
64. Chatterjee, P.; Chakraborty, S. Material selection using preferential ranking methods. *Mater. Des.* **2012**, *35*, 384–393. [CrossRef]

65. Erdogan, S.; Aydin, S.; Balki, M.K.; Sayin, C. Operational evaluation of thermal barrier coated diesel engine fueled with biodiesel/diesel blend by using MCDM method base on engine performance, emission and combustion characteristics. *Renew. Energy* **2020**, *151*, 698–706. [CrossRef]
66. Darji, V.P.; Rao, R.V. Intelligent multi-criteria decision making methods for material selection in sugar industry. *Procedia Mater. Sci.* **2014**, *5*, 2585–2594. [CrossRef]
67. Siregar, D.; Arisandi, D.; Usman, A.; Irwan, D.; Rahim, R. Research of simple multi-attribute rating technique for decision support. *J. Phys. Conf. Ser.* **2017**, *930*, 012015. [CrossRef]
68. Patel, M.R.; Vashi, M.P.; Bhatt, B.V. SMART-Multi-criteria decision-making technique for use in planning activities. In Proceedings of the New Horizons in Civil Engineering, Surat, India, 25–26 March 2017.
69. Rao, R.V.; Singh, D. Evaluating flexible manufacturing systems using euclidean distance-based integrated approach. *Int. J. Risk Manag.* **2012**, *3*, 32–53. [CrossRef]
70. Rao, R.V.; Singh, D. Weighted Euclidean distance-based approach as a multiple attribute decision making method for plant or facility layout design selection. *Int. J. Ind. Eng. Comput.* **2012**, *3*, 365–382.
71. Alinezhad, A.; Khalili, J. *New Methods and Applications of Multiple Attribute Decision Making (MADM)*; Springer Nature: Berlin/Heidelberg, Germany, 2019; p. 193.
72. Tesic, D.; Radovanovic, M.; Bozanic, D.; Pamucar, D.; Milic, A.; Puska, A. Modification of the DIBR and MABAC methods by applying rough numbers and its application in making decisions. *Information* **2022**, *13*, 353. [CrossRef]
73. Chakraborty, S. Applications of the MOORA method for decision making in manufacturing environment. *Int. J. Adv. Manuf. Technol.* **2011**, *4*, 1155–1166. [CrossRef]
74. Dominguez, L.P.; Mojica, K.Y.S.; Pabon, L.C.O.; Diaz, M.C.C. Application of the MOORA method for the evaluation of the industrial maintenance system. *J. Phys. Conf. Ser.* **2018**, *1126*, 012018. [CrossRef]
75. Triantaphyllou, E.; Shu, B.; Sanchez, S.N.; Ray, T. Multi-criteria decision making: An operations research approach. In *Encyclopedia of Electrical and Electronics Engineering*; Webster, H.G., Ed.; John Wiley & Sons: New York, NY, USA, 1998; Volume 15, p. 175.
76. Deng, H.; Yeh, C.H.; Willis, R.J. Inter-company comparison using modified TOPSIS with objective weights. *Comput. Oper. Res.* **2000**, *27*, 963–973. [CrossRef]
77. Gul, M.; Celik, E.; Aydin, N.; Gumus, A.T.; Guneri, A.F. A state of the art literature review of VIKOR and its fuzzy extensions on applications. *Appl. Soft Comput.* **2016**, *46*, 60–89. [CrossRef]
78. Sayadi, M.M.; Heydari, M.; Shahanaghi, K. Extension of VIKOR method for decision making problem with interval numbers. *Appl. Math. Model.* **2009**, *33*, 2257–2262. [CrossRef]
79. Mohanty, P.P.; Mahapatra, S.S. A compromise solution by VIKOR method for ergonomically designed product with optimal set of design characteristics. *Procedia Mater. Sci.* **2014**, *6*, 633–640. [CrossRef]
80. Trung, D. Multi-criteria deciison making under MARCOS method and weighting methods: Applied to milling, grinding, and turning processes. *Manuf. Rev.* **2022**, *9*, 3.
81. Stevic, Z.; Pamucar, D.; Puska, A.; Chatterjee, P. Sustainable supplier selection in healthcare insudtries using a new MCDM method: Measurement Alternatives and Ranking according to Compromise Solution (MARCOS). *Int. J. Appl. Eng. Res.* **2020**, *140*, 106231.
82. Levine, M.; Ramsey, P.P.; Smidt, R.K. *Applied Statistics for Engineers and Scientists*; Prentice-Hall: Upper Saddle, NJ, USA, 2001.
83. Navidi, W. *Statistics for Engineers and Scientists*, 3rd ed.; McGraw-Hill Science/Engineering: New York, NY, USA, 2010.